Distribution Agreement

In presenting this thesis or dissertation as a partial fulfillment of the requirements for an advanced degree from Emory University, I hereby grant to Emory University and its agents the non-exclusive license to archive, make accessible, and display my thesis or dissertation in whole or in part in all forms of media, now or hereafter known, including display on the world wide web. I understand that I may select some access restrictions as part of the online submission of this thesis or dissertation. I retain all ownership rights to the copyright of the thesis or dissertation. I also retain the right to use in future works (such as articles or books) all or part of this thesis or dissertation.

Signature:

Carson R. Powers	Date

An Investigation of Methanol Photolysis Branching Ratios and Their Implications for Chemistry in the Interstellar Medium

By

Carson R. Powers
Master of Science
Chemistry

Susanna L. Widicus Weaver, Ph.D
Advisor

Dr. Michael C. Heaven, Ph.D
Committee Member

Dr. James T. Kindt, Ph.D
Committee Member

Accepted:

Lisa A. Tedesco, Ph.D
Dean of the James T. Laney School of Graduate Studies

Date

An Investigation of Methanol Photolysis Branching Ratios and Their Implications for Chemistry in the Interstellar Medium

By

Carson R. Powers
B.S., College of William and Mary, 2015

Advisor: Susanna L. Widicus Weaver, Ph.D

An abstract of
a thesis submitted to the Faculty of the
James T. Laney School of Graduate Studies of Emory University
in partial fulfillment of the requirements for the degree of
Master of Science
in Chemistry
2018

Abstract

An Investigation of Methanol Photolysis Branching Ratios and Their Implications for Chemistry in the Interstellar Medium

By Carson R. Powers

Methanol is ubiquitous in star-forming regions, and recent astrochemical models have shown that methanol photolysis contributes largely to more complex organic chemistry which occurs in interstellar ices. While some of the branching ratios for methanol photolysis have been measured via mass spectrometric techniques, the photolysis products methoxy (CH_3O) and hydroxymethyl (CH_2OH) cannot be distinguished using these methods. Additionally, recent experiments focused on the photoprocessing of interstellar ice analogues have led to conflicting theories about the branching ratios because the radical products can undergo further reactions in the ice matrix. To address these challenges, we have implemented pure rotational spectroscopy in the millimeter and submillimeter regimes to quantitatively probe the products of methanol photolysis. We conduct experiments in the gas phase, where the photoproducts can be stabilized in a supersonic expansion, and secondary reactions of the radical photolysis products can be minimized. We use a UV excimer laser to dissociate methanol near the throat of a supersonic expansion, and probe the products after they have undergone sufficient rotational cooling. Rotational diagram analysis is then performed with collected spectra to determine the relative density of each photolysis product relative to methanol. We have thus far detected formaldehyde, methoxy, hydroxymethyl, and carbon monoxide as products of methanol photolysis. We present here the experimental setup and the initial results for methanol photolysis branching ratios. Additionally, production of isotopic formaldehyde as a photolysis product, and detection of water are discussed, as are future directions for the project.

An Investigation of Methanol Photolysis Branching Ratios and Their Implications for Chemistry in the Interstellar Medium

By

Carson R. Powers
B.S., College of William and Mary, 2015

Advisor: Susanna L. Widicus Weaver, Ph.D

A thesis submitted to the Faculty of the
James T. Laney School of Graduate Studies of Emory University
in partial fulfillment of the requirements for the degree of
Master of Science
in Chemistry
2018

Acknowledgement

It is hard to know where to begin here, when I have so many people to be thankful for. I suppose I will start with the members of my own lab, which naturally begins with Susanna.

Dr. Susanna Widicus Weaver took me on as a student in the summer of 2015, when I heard about her astrochemistry lab, and wished to learn more about it. That summer, I gathered just how hands on a laboratory focused on gas phase spectroscopy can be, but I enjoyed my time during that summer rotation, and knew that enjoying my work would factor largely in how successful I would be in graduate school. I was extremely happy to find out at the end of that fall that she was willing to take me on as a student, and my journey into investigating the branching ratios of gas phase methanol photolysis began there. Susanna, I'll always appreciate the fervor and excitement with which you approach the science that is conducted in the lab. I've also enjoyed the honest conversations we've been able to have, and the guidance which you've provided through these talks. Above all else, I appreciate the opportunity you've provided me by allowing my continued growth and development as a scientist and a person. All I can offer here is a simple thank you, but know that any success I achieve in the future is owed in part to my time in the Widicus Weaver lab. Thank you, Susanna.

There have been many colleagues who have come and gone in the Widicus Weaver lab during my three years at Emory. I first learned about the spectrometer I've worked on all this time from Dr. Brian Hays and Morgan McCabe, who left me with the general tools and knowledge to begin pushing science forward on my own. Dr. Luyao Zou was a good friend who taught me many things, most notably the power of code, a love of Linux, and to investigate the math corresponding to the spectroscopy being conducted. AJ Mesko was one of the most genuinely nice people I had the fortune of knowing at Emory, and was always up to the challenge of cheering up anyone around him. Kevin Roenitz and I joined the Widicus Weaver lab at the same time, and he immediately hovered towards the instrumentation the lab had to offer. I admire his ability to engineer creative solutions to complex problems in spectrometer design, and know he will be successful as he pushes forward in the lab towards the doctorate. Our three newest students, Hayley Bunn, Connor Wright, and Katarina Yocum have brought new life into the group, and I'm excited to hear how they will grow and develop into great scientists in their own right during their time at Emory. Previous postdoctoral fellow Dr. James McMillan offered helpful conversation and insight in regards to spectroscopy and data analysis, as well as a great set of lab hands and repertoire of puns.

Outside of the lab, I'd like to thank the other members of my committee, Dr. Michael Heaven and Dr. James Kindt, for their help and support in classes, research, and in the editing of this very document. A special thank you to Steve Krebs and Claire Scott for always being in our corner when it came to getting purchases for the lab, and fighting on our behalf when something was unreasonably late in being delivered. To all of my friends in the chemistry department, my girlfriend Alexia, as well as my undergraduate companions in the acapella group AHANA, you helped to

keep me grounded outside of the lab, a feat which is by no means simple, and deserves mention.

Lastly, I'd like to thank my family, and especially my mother and father for always having open ears and open hearts to my troubles and concerns, whether they were related to my journey through graduate school or not. Everything I do, I do for you two; I love you very much.

Table of Contents

List of Figures

List of Tables

Chapter 1 Introduction

1.1 General Introduction to the ISM

The interstellar medium (ISM) consists of many types of environments and locations which are rife with chemistry, involving neutral molecules, ions, and radicals alike. Current astrochemical models theorize that chemistry takes place in two distinct ways: in the gas phase, which depending on the region in the ISM might contain a low number density of molecules [1]; and also on the surface of icy grains, which are typically carbonaceous or silicate grains coated with a few monolayers of water containing trace amounts of CO, NH_3, and small organic molecules, such as H_2CO and CH_3OH [2, 3]. However, around 200 molecules have been detected in the ISM, in gases and in ices[1]. All molecules which are found in the ISM may play a larger part in chemistries which lead to the start of life, and understanding the number densities, spatial distributions, and temperatures of molecules in these different regions allows us insight into how larger complex organic molecules (COMs) might form.

Much of the challenge in astrochemistry arises from attempting to explain the formation pathways for the creation of observed COMs, because they are not well understood. For many years, it was believed that gas-phase ion-molecule reactions were the main routes to the production of many of the complex species observed in the ISM [4–6]. However, these reaction routes have not explained the abundances of certain complex organic molecules in the gas phase [7]. In recent years, gas-grain chemistry has been proposed as an explanation for the production of these COMs. In this regard, recent astrochemical models have attempted to include the formation of COMs via UV photolysis of icy mantles and the small organics which compose them,

[1] http://www.astro.uni-koeln.de/cdms/molecules

followed by radical-radical recombination reactions on the grain surface [2, 8, 9].

Regardless of the ways these molecules are created, the original question remains: What tools are available to know what molecules are present in the gas phase in the ISM? The answer is a technique which has been implemented by observational astronomers for over half a century [10], but has become a powerful tool for scientists in the lab: Rotational spectroscopy.

Portions of this thesis have been reproduced and/or amended from the following source:

- S. L. Widicus Weaver, C. R. Powers, M. N. McCabe, S. Zinga *Proc. of Astrochemistry VII*, 332 (2017). 2017 Intl. Astronomical Union Symp.

1.2 Methanol Photolysis, and Branching Ratios in the ISM

Of the small organic molecules which make up interstellar ices, methanol has a high fractional abundance in dense molecular cores, in some cases making up between 15 - 20% of the total composition [11]. Photolysis of methanol in these ices is believed to be a major contributor to the number density of small organic radicals which have the potential to create most of the COMs observed in the ISM [2]. The photolysis mechanism for methanol can occur via several reaction pathways, determined both experimentally and by theory [12–16], which can be seen below in Equation 1.1:

$$\begin{aligned} CH_3OH &\rightarrow CH_2 \ + H_2O \\ &\rightarrow HCOH + H_2 \\ &\rightarrow CO + 2H_2 \\ &\rightarrow CH_3 + OH \\ &\rightarrow CH_2O + H_2 \\ &\rightarrow CH_3O + H \\ &\rightarrow CH_2OH + H \end{aligned} \tag{1.1}$$

In terms of relative energies for dissociation via individual pathways, a reaction energy diagram can be seen in Figure 1.1. The radicals methoxy (CH_3O) and hydroxymethyl (CH_2OH), in particular, are of great interest to the astrochemical community. Further reaction of these radicals with hydroxyl radical (HCO), which is readily produced from the photolysis of formaldehyde, can lead to the production of either glycolaldehyde or methyl formate, two structural isomers with the formula $C_2H_4O_2$.

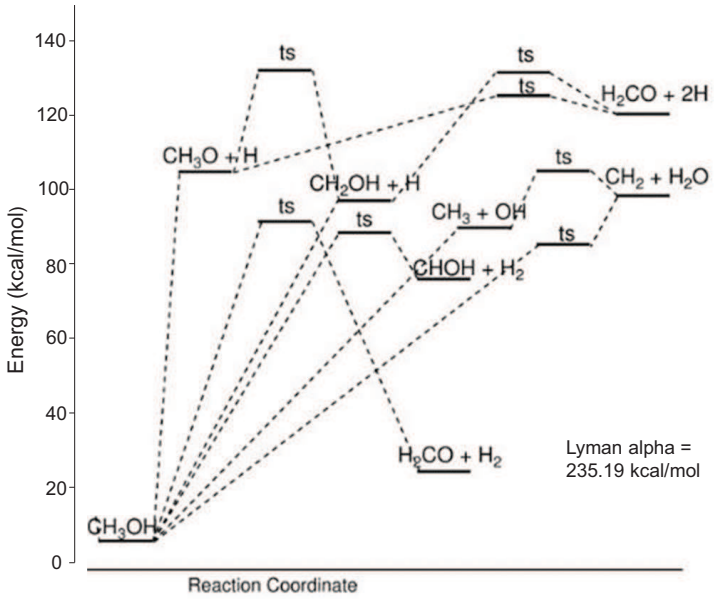

Figure 1.1: The different reaction pathways for methanol photolysis.

In the modeling work performed by Garrod et al., methanol photolysis offers

plausible explanations to formation routes of these COMs in order to explain the differing abundances observed in interstellar molecular sources. Hence, trying to measure and determine the exact branching ratios for as many pathways as possible is desired by many astrochemists.

Hagege et al. were the first to experimentally measure branching ratios for the gas-phase photolysis of methanol using a mercury/neon lamp emitting at 184.9 nm, and analyzing the results using mass spectrometry [15]. Results for a few of the photolysis pathways were gathered from this experiment; these can be seen in Equation 1.2. Unfortunately, because mass spectrometry does not allow for differentiation between species of the same mass, it is impossible to tell from these results which radical (methoxy or hydroxymethyl) is the major product; only that they make up the majority of what is produced.

$$\left.\begin{aligned} CH_3OH \rightarrow CH_3O \text{ (or } CH_2OH) + H \end{aligned}\right\} \sim 75\%$$
$$\left.\begin{aligned} \rightarrow CH_3 + OH \end{aligned}\right\} \sim 5\% \qquad (1.2)$$
$$\left.\begin{aligned} \rightarrow CH_2O + H_2 \end{aligned}\right\} \sim 20\%$$

More than 40 years later, Öberg et al. performed experiments involving both reflection-absorption infrared spectroscopy (RAIRS) and mass spectrometry to observe and characterize the COMs which are produced in the condensed phase during radical recombination after UV irradiation, as well as controlled rates of temperature programmed desorption (TPD)[16]. This study also determined that the two radicals of interest made up the majority of the photolysis products; more specifically, this study stated that hydroxymethyl was the main radical produced via photolysis on the grain surface. However, the researchers back-calculated the branching ratios for these channels using a model which only considers the first generation dissociation and recombination of radicals for methanol, and no direct observation of radicals produced

in the ice was reported.

Gas phase spectroscopy probing the products of methanol photolysis offers a way to elucidate the branching ratios of the photolysis mechanism by identifying the products through their pure rotational transitions. Using methods similar to those used in observational radio astronomy, the densities and temperatures of each product channel can be determined through a Boltzmann analysis, and branching ratios can be calculated. To this end, the experiments performed in this work were aimed at attempting to collect direct, quantitative measurements of the photolysis products of methanol using millimeter/submillimeter rotational spectroscopy.

Chapter 2 Experimental Setup

The methanol photolysis experiment utilized several pieces of equipment to facilitate the production and detection of photolysis products, specifically radical species. The generation of mm/submm light is achieved via microwave radiation in the range of 0 - 50 GHz produced by a frequency synthesizer (Agilent Technologies, E8257D PSG with options 1EA, UNU, 550, and UNT) that is then multiplied to a range of 70 - 1000 GHz using frequency multipliers to generate harmonics of this light (Virginia Diodes Inc., AMC-S268). The resultant light is passed through a sample, and subsequently detected using an InSb hot electron bolometer (QMC Ltd., QFI/XBI), where the voltage output is collected using a digital oscilloscope (National Instruments, PCI-5124). The molecules were introduced to the probing radiation inside a supersonic expansion, a technique in which species of interest are seeded into a buffer gas that enters a vacuum through a small orifice; the pressure differential leads to an adiabatic expansion of molecules into the vacuum chamber, where collisions between the dilute seed molecules and buffer gas cause the internal rotational and vibrational energy of the molecules to transfer to translational motion of the buffer gas parallel to the direction of the expansion. Because of the degree of cooling this leads to, molecules have a limited number of rotational and vibrational states that can be populated, which leads to fewer and stronger rotational transitions to be probed. This technique also helps quench the excess energy which could cause species to dissociate, making it useful for ensuring the survival of radical products.

The supersonic expansion in this experiment was implemented by flowing argon gas at 32 psig through a bubbler which contained HPLC grade liquid methanol. The gas mixture flowed through a pulsed valve (Parker Hannifin, Series 9) with an aperture exit 1 mm in diameter at a rate of 44 Hz and valve open time of 2 ms, into a vacuum

chamber evacuated to a background pressure between 10-12 mTorr by a roots blower pump (Oerlikon Leybold Vacuum, Ruvac WSU-2001) with a pumping speed of 2000 L sec^{-1} backed by a rotary vane pump (Oerlikon Leybold Vacuum, Sogevac SV630 B) with a pumping speed of 250 L sec^{-1}. A flow controller (MKS 1179A, 5000 sccm) connected to a four channel flow rate readout (MKS Type 247) was used to monitor and adjust the gas flowing into the vacuum chamber, maintaining constant stagnation pressure.

A UV excimer laser (GAM LASER Inc., EX5 250 Hz) produced light at 193 nm, which was passed through a spherical focusing lens (Thorlabs, ⌀1" UVFS Plano-Convex Lens, f=750.0 mm) before propagating into the vacuum chamber. At the focal length of the lens, the light hit a fused silica tube (Wilmad-LabGlass) containing the gas mixture; the distance between the laser spot and the expansion into the vacuum can be optimized for each experiment.

In an effort to improve the signal-to-noise ratio (SNR) of spectra produced, a multipass optical cavity constructed from a set of two spherical mirrors (Edmund Optics, 15.24 cm diameter and 15.24 cm focal length, NT32-836) was implemented to increase the pathlength of radiation through the sample in the supersonic expansion. The construction of this cavity lead to a setup which provided seven passes through the center of the chamber, and is based on the design created by Kaur et al. [17]. The full experimental setup can be seen in Figure 2.1.

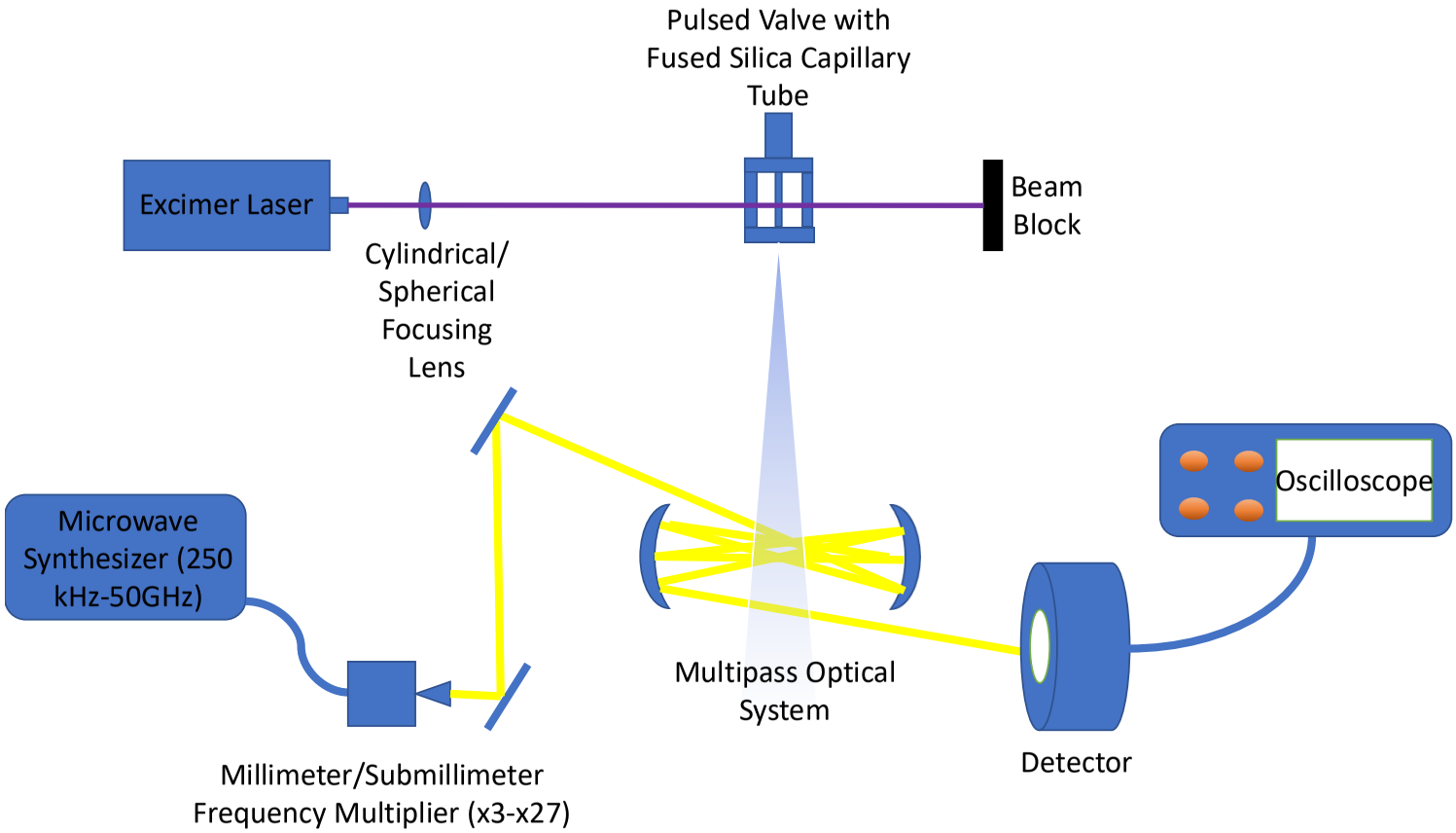

Figure 2.1: Experimental setup in the vacuum chamber.

Chapter 3 Results and Summary

3.1 Methanol Photolysis

3.1.1 Rotational Diagram Analysis

The rotationally resolved spectra collected during the course of this experiment are analyzed using a Boltzmann diagram analysis, implementing the method described by Laas et al. [18]. This analysis allows for the determination of the absolute rotational temperature of molecules, as well as their relative abundance ratios, by integrating over the intensity of several observed spectral lines for each molecule detected and then examining the relationship between the upper state energies of each transition and the line intensities through the following equation:

$$\int_{-\infty}^{\infty} I_{\mathrm{b}}\,\mathrm{d}\nu = \frac{hc^3 A g_{\mathrm{u}}}{8\pi k \nu^2}\frac{N_{\mathrm{T}}}{Q(T_{\mathrm{rot}})}\mathrm{e}^{-E_{\mathrm{u}}/kT_{\mathrm{rot}}} \tag{3.1}$$

In this equation, h is Planck's constant, k is Boltzmann's constant, A is the Einstein-A coefficient for the transition, g_{u} is the upper state degeneracy, ν is the transition frequency, N_{T} is the column density, $Q(T_{\mathrm{rot}})$ is the rotational partition function, and T_{rot} is the rotational temperature of the molecule. Since we are measuring an absorption process, the Einstein-A coefficient is substituted out for the Einstein-B using the following relationship:

$$A_{1\rightarrow 0} = B_{1\leftarrow 0}\frac{8\pi h\nu^3}{c^3} \tag{3.2}$$

Likewise, the lower state energies for the transitions must be used, and can be substituted into the Boltzmann factor using the relationship $E_{\mathrm{u}} = E_{\mathrm{l}} + h\nu$. The lower state energies, as well as the frequencies for the absorption lines, were obtained from the Jet Propulsion Lab (JPL) Molecular Spectroscopy database [19]. Plotting

$\ln[(\int_{-\infty}^{\infty} I_{\mathrm{b}} \mathrm{d}\nu)(\mathrm{k}/(h^2 \nu B g_{\mathrm{u}}))]$ on the y-axis and E_{l} on the x-axis will create a linear plot where the slope is inversely proportional to the T_{rot} of the molecules, and the intercept equal to $\ln(N_{\mathrm{T}}/Q(T_{\mathrm{rot}}))$. The spectral intensities are not calibrated to number density in this experiment. Nonetheless, the N_T calculated from the y-intercept can be used to find the relative abundance ratio of each product channel to the methanol parent molecule.

3.1.2 Spectral Roadmap

It was known that the photolysis products observed in this experiment would be rotationally cooled, due to the use of a supersonic expansion implemented in the spectrometer design. This meant a decrease in the rotational partition function, leading to a smaller amount of rotational states which could be accessed, and therefore an increase in the SNR of spectra which would be collected. This, however, also meant that the number of lines which could be experimentally observed was small, and when looking through lists of lines on the Jet Propulsion Lab (JPL) and Cologne Database for Molecular Spectroscopy (CDMS), attention needed to be given to not only the line strength for a particular transition, but also the energy for the lower state involved in the transition.

It was also discovered that when attempting to scan for radicals with very weak SNR, picking the strongest transition would be necessary to not only give the best chance at seeing the production of these species of interest, but to also potentially decrease the amount of time needed to average a signal. To this end, it was necessary to develop a strategy for targeting the strongest rotational transitions, given an assumed rotational temperature.

In order to calculate and compare the relative intensities for transitions of a molecule at a specific temperature, it is useful to define and understand several spectroscopic concepts. First, we need to understand Beer's Law, which allows for the

calculation of a power P measured from a detector after having interacted with a sample at an incident power P_0. The equation for Beer's Law can be written as

$$P = P_0 e^{-A} \tag{3.3}$$

The truly important variable to understand and define here is A, which is known as absorbance. The value for absorbance is intrinsically tied to the frequency at which a transition for a sample occurs, the probability that a photon will be absorbed at that frequency, the energy attributed with the lower state involved in the transition, the temperature of the system, and the rotational partition function for the molecule. Absorbance can be fully defined using the following equation:

$$A = (\frac{8\pi^3}{3hc})(\frac{nL}{Q(T)})v_0(1 - \exp[-\frac{hv_0}{k_B T}])\exp[-\frac{E_L}{k_B T}]S \tag{3.4}$$

In Equation 3.4, h is Planck's constant, c is the speed of light, n is the total number density of absorbing species, L is the total length of the region in which absorption occurs, $Q(T)$ is the rotational partition function for a species at a certain temperature, v_0 is the frequency associated with the transition for the species, k_B is the Boltzmann constant, T is the temperature of the sample being probed, E_L is the energy associated with the lower state of the molecule involved in the transition, and S is the line strength associated with a transition, which can be extracted from the Einstein absorption coefficient B for a transition, defined as

$$B = (\frac{8\pi^3}{3h^2})|\langle\Psi_n|\overrightarrow{\mu}|\Psi_m\rangle|^2 \tag{3.5}$$

The information required for calculating the absorbance of a transition can be obtained from information provided in the JPL catalog for specific molecules [19].

An Igor procedure file written by Dr. Ivan Medvedev and Dr. Christopher Neese during their time in the De Lucia lab circa 2010 at Ohio State can be used to quickly and accurately calculate the absorption of molecular transition, known as CAAARS

(Computer Aided Assignment of Asymmetric Rotor Spectra). Using the linelist information from JPL (or CDMS), generation of a "spectral roadmap" was possible, which aided in picking transitions for which to search, assuming the molecules were sufficiently cooled by the supersonic expansion. To this end, the JPL and CDMS documentation provides partition function information for several specific temperatures for every molecule listed. For the work presented herein, a rotational temperature of 37.50 K (and the corresponding partition function) were used in the calculation of these absorbance intensity values. An example of spectral predictions generated using CAAARS for methanol lines in Band 5 can be seen in Figure 3.1. While a

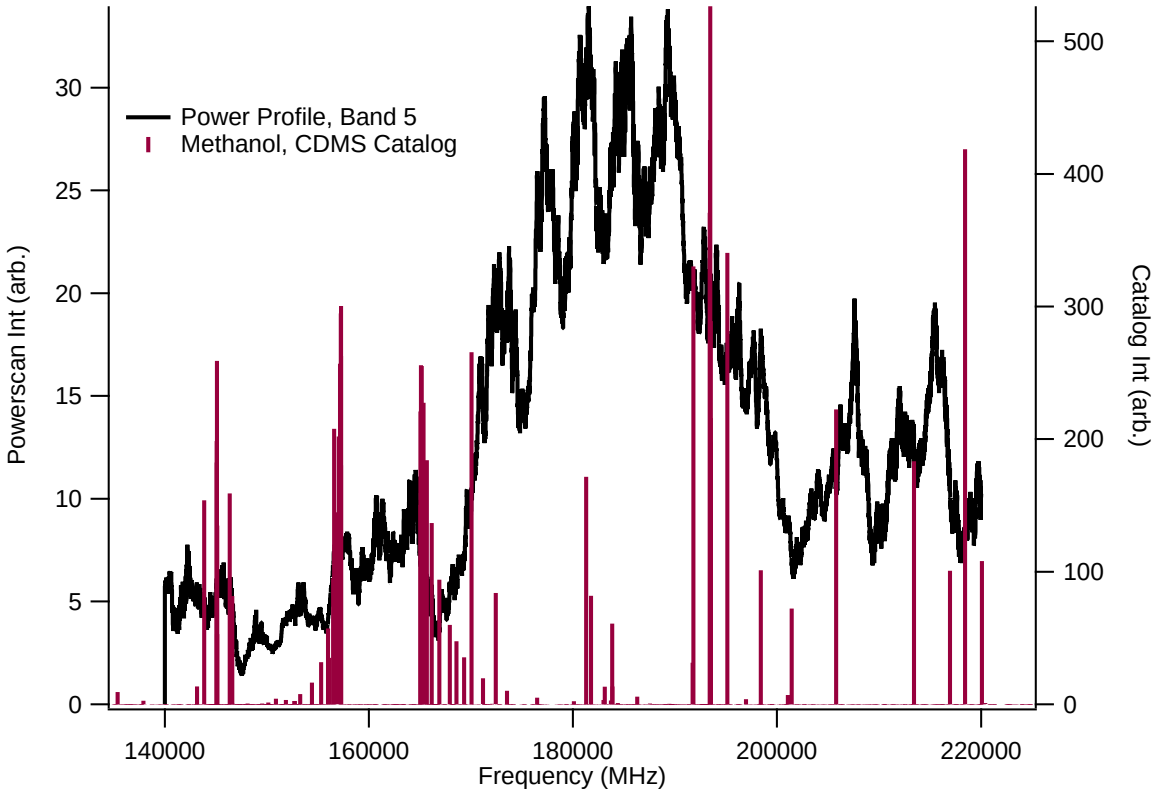

Figure 3.1: A spectrum showing generated intensities for transitions of methanol with Q(37.50 K), overlaid with the power profile for Band 5 generated from the AMC-S268 multiplier chain. Arbitrary intensities for the AM power profile and the transitions from the catalog can be found on the left and right vertical axes, respectively.

transition itself may be inherently strong, it may fall in a very unfavorable region of power output for the multiplier chain. In order to get a much clearer idea of which

transitions would be best to target with the equipment at our disposal, it is better to take the calculated catalog intensities, and multiply them by the observed intensity output at the transition frequency for the amplitude modulated (AM) power profile. This adjusted value for the intensity of a transition can more accurately guide which transitions should be targeted for scanning, and save a researcher valuable time. Below in Figure 3.2, it can be seen for the transitions between 135-140 GHz that the stronger transitions in that range suffer because of the poor power output (which is virtually nonexistent) from the multiplier chain at that range. Based on these calcu-

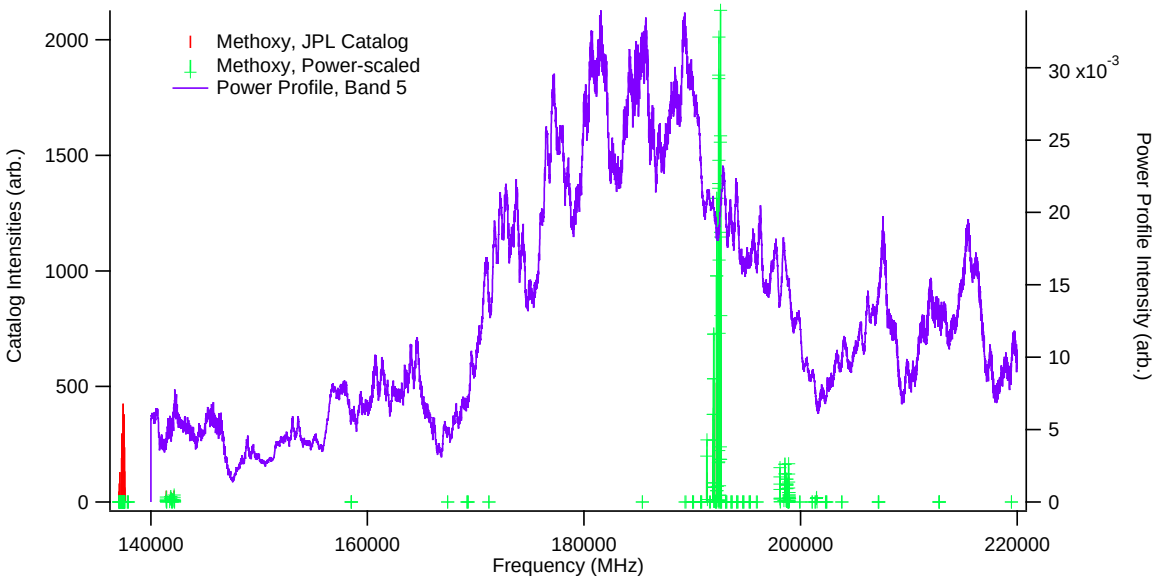

Figure 3.2: A spectrum which shows the power-scaled intensities for methoxy versus catalog intensities generated using CAAARS

lations (and general constraints based on the amount of lines available for particular molecules), I have been able to confirm and target the best candidate transitions for the molecules I have attempted to detect. Table 3.1 shows a list of these transitions for methanol and the photolysis products formaldehyde and methoxy. An important factor to note is that not all of these transitions were targeted every time the experiment was performed. Time constraints, in regards to averaging, prohibited this in the beginning stages of the experiment.

Table 3.1: A list of transitions targeted for the parent molecule, methanol, and the photolysis products investigated during the course of this experiment. The Einstein A coefficients for hydroxymethyl are provided from a fit made using parameters from Reference [24].

Molecule	Frequency (MHz)	Einstein A Coefficient	Quantum Numbers ($J^{\pm}_{K_A K_C}$)
Methanol	145,093.754	$1.22*10^{-5}$	$3^{+}_{0,3}$ - $2^{+}_{0,2}$
	145,097.435	$1.08*10^{-5}$	$3^{-}_{1,2}$ - $2^{-}_{1,1}$
	145,103.185	$1.22*10^{-5}$	$3^{+}_{0,3}$ - $2^{+}_{0,2}$
	145,131.864	$1.11*10^{-5}$	$3^{+}_{1,2}$ - $2^{+}_{1,1}$
	165,050.175	$2.32*10^{-5}$	$1^{+}_{1,0}$ - $1^{+}_{0,1}$
	193,454.358	$6.59*10^{-6}$	$4^{+}_{0,4}$ - $3^{+}_{0,3}$
Formaldehyde	140,839.502	$5.24*10^{-5}$	$2_{1,2}$ - $1_{1,1}$
	145,602.949	$7.72*10^{-5}$	$2_{0,2}$ - $1_{0,1}$
	150,498.334	$6.39*10^{-5}$	$2_{1,1}$ - $1_{1,0}$
	211,211.468	$2.23*10^{-4}$	$3_{1,3}$ - $2_{1,2}$
	218,222.192	$2.77*10^{-4}$	$3_{0,3}$ - $2_{0,2}$
Methoxy	192,434.201	$1.50*10^{-4}$	$3_{0,1}$ - $2_{0,0}$
	192,451.014	$1.31*10^{-4}$	$3_{1,0}$ - $2^{-}_{1,0}$
	192,600.454	$7.51*10^{-5}$	$3_{2,0}$ - $2_{2,0}$
	192,615.976	$1.17*10^{-4}$	$3^{-}_{1,0}$ - $2_{1,0}$
Hydroxymethyl	210,922.652	$2.90*10^{3}$	$6_{1,5}$ - $6_{0,6}$
	227,604.358	$1.50*10^{-4}$	$7_{1,6}$ - $7_{0,7}$
Carbon Monoxide	230,538.000	$6.78*10^{-7}$	2 - 1
	461,040.768	$5.91*10^{-6}$	4 - 3
	576,267.930	$1.17*10^{-5}$	5 - 4
Water	183,310.087	$3.54*10^{-6}$	$3_{1,3}$ - $2_{2,0}$
	556,935.987	$3.28*10^{-4}$	$1_{1,0}$ - $1_{0,1}$

3.1.3 Initial Detection of Methanol, and Calculation of a Rotational Energy Diagram

Using the original spectrometer design described in reference [20], laser photolysis was conducted on a gas mixture containing methanol vapor seeded in argon, and the subsequent supersonic expansion was probed using microwave light at Band 5 (140-220 GHz). This design can be seen in Figure 3.3.

The methanol depletion signal, shown in Figure 3.4, is an indication of successful photolysis, and manifests as a decrease in a methanol absorption signal [21]. The depletion signal confirmed that searches for photodissociation products of methanol could be undertaken.

To start the experiment on a given day, several methanol absorption lines are measured in the absence of laser light. Figure 3.5 shows two spectra which were collected before the implementation of the multipass optical system. Spectra seen in Figure 3.6 are methanol spectra which were collected after implementation of the multipass optical setup in the spectrometer.

Typically, absorption lines in spectra collected via direct absorption spectroscopy have a Gaussian lineshape, and we would fit these data with a Gaussian function to determine the integrated line intensity. However, because of both the asymmetric lineshape of the features and the baseline difference on either side of the absorption lines, fitting a pure Gaussian function is not accurate, and leads to error when attempting to determine the area underneath the absorption peak. The reason for the asymmetric lineshape is unknown, but it is suspected to arise from an instrumentation or software artifact because it is also seen in other experiments conducted using similar, but not identical, instrumentation in our laboratory.

One way to avoid the confusion of assigning a Gaussian fit to these absorption lines is to simply take the peak of an absorption line, and assume it is proportional to the integrated intensity from Equation 3.1. This assumption is valid if the veloc-

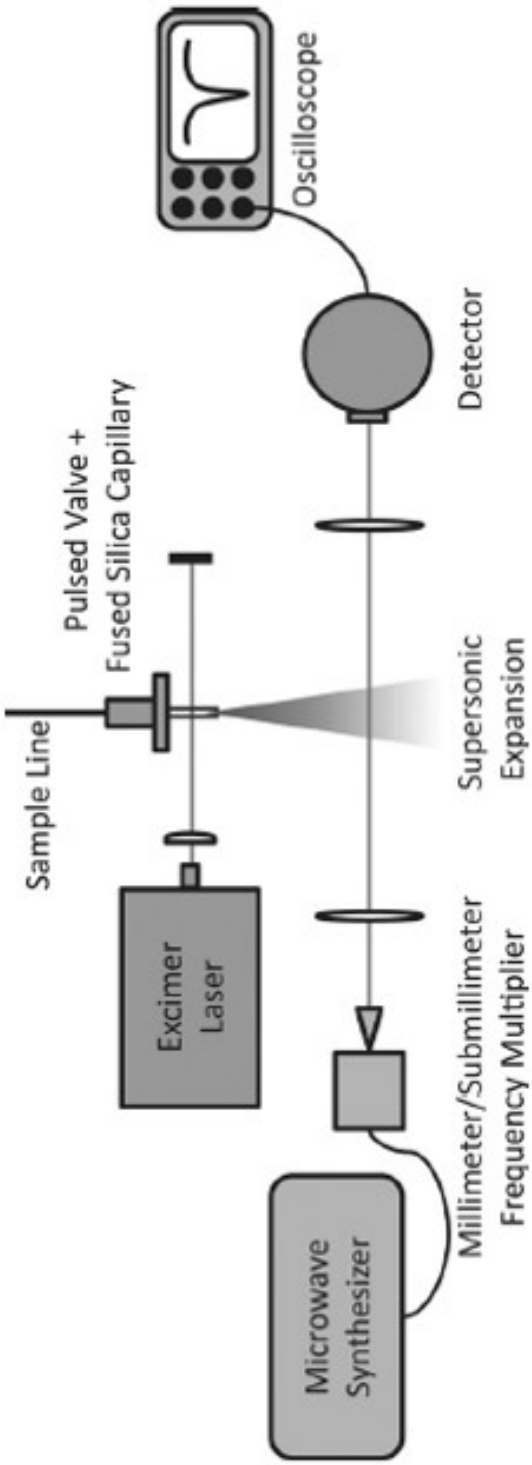

Figure 3.3: The design of the spectrometer used in conducting $O(^1D)$ insertion experiments, and in the early stages of the methanol photolysis project. Figure from Reference [20].

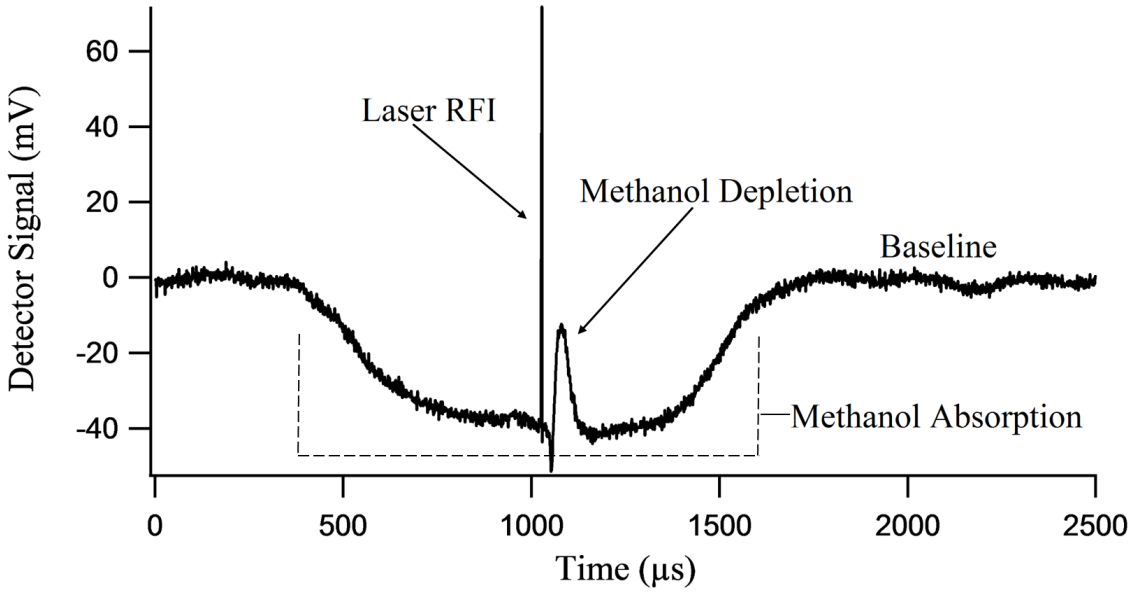

Figure 3.4: A methanol depletion signal caused by photolysis via the UV excimer laser. The absorption feature on this plot and spectra of absorption features (in terms of signal intensity) can be quantified as $I\text{-}I_0$, where I is the intensity of light detected after absorption by methanol, and I_0 is the intensity of the incident light. Figure from Reference [21].

ity component of the Doppler linewidth is consistent across absorption lines for one molecule; as long as the pulsed valve is in good working condition, this should be true. This is based on the adiabatic properties of the supersonic expansion; collisions in the gas lead to a velocity distribution for any particular molecule which approaches an equilibrium. We also assume that the asymmetry seen in lines mentioned earlier is consistent for every spectra. When performing a Boltzmann diagram analysis, whether using the peak intensity or the integrated intensity, the slope for a given molecule, and the ratio of y-intercepts between molecules will not change.

In order to properly analyze the results, uncertainty needs to be assigned for the line peaks used in subsequent calculations. For this, the RMS noise value for a region of baseline to the left of each absorption line was calculated. The baseline to the left of the signal was chosen as the reference for the determination of the RMS noise value, as the scan goes from lower frequency (to the left) to higher frequency (to the

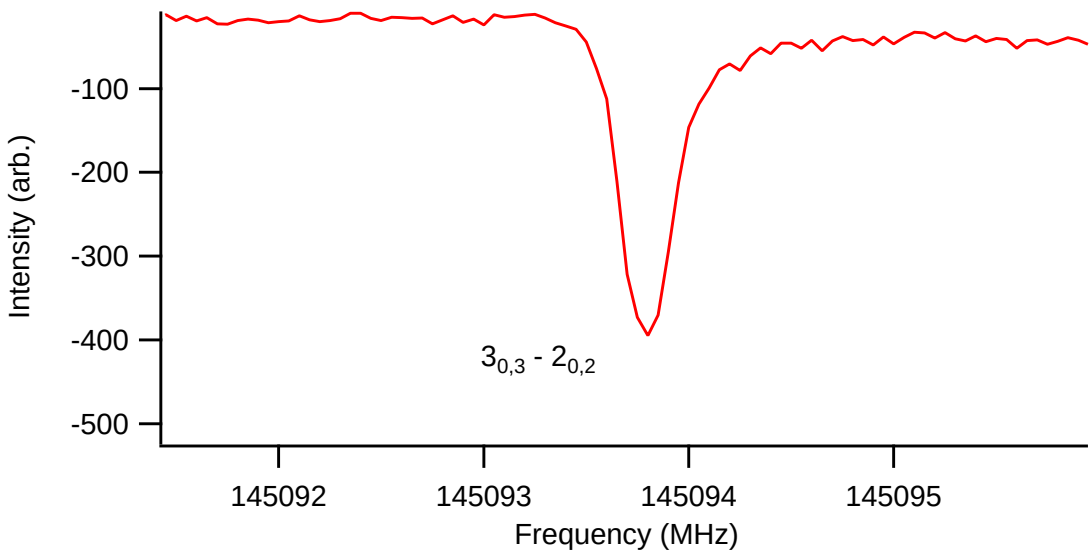

(a)

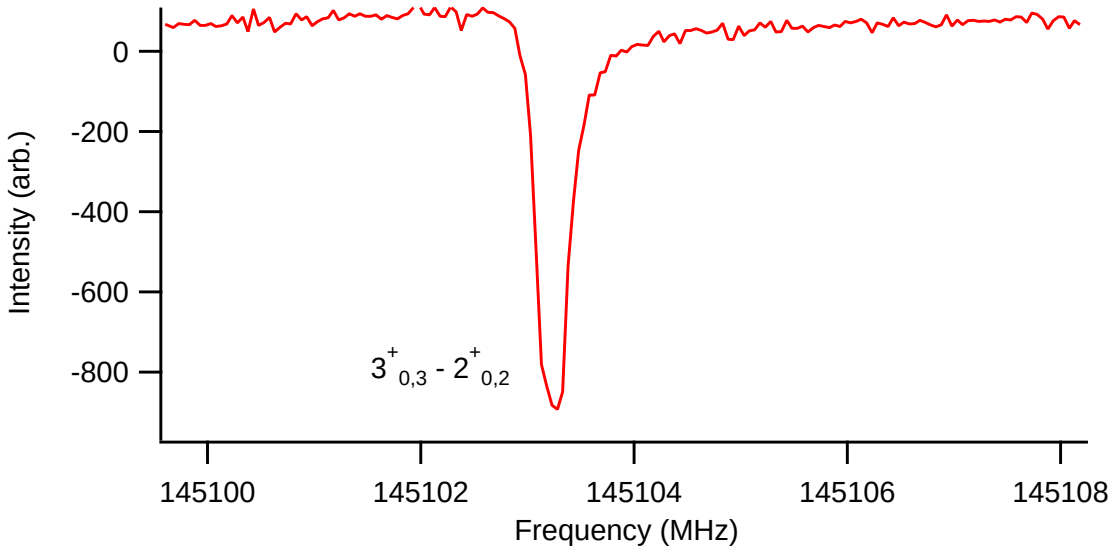

(b)

Figure 3.5: Two examples of methanol spectra, with their assigned rotational quantum numbers. Because the number density of methanol in the expansion is not known, the intensity units can not be quantified; therefore, the intensity units are an arbitrary voltage value. (a) The methanol absorption signal at 145,093.754 MHz, with the rotational quantum number assignment $3_{0,3}$-$2_{0,2}$; and (b) The methanol absorption signal at 145,103.185 MHz, with the rotational quantum number assignment $3^{+}_{0,3}$-$2^{+}_{0,2}$.

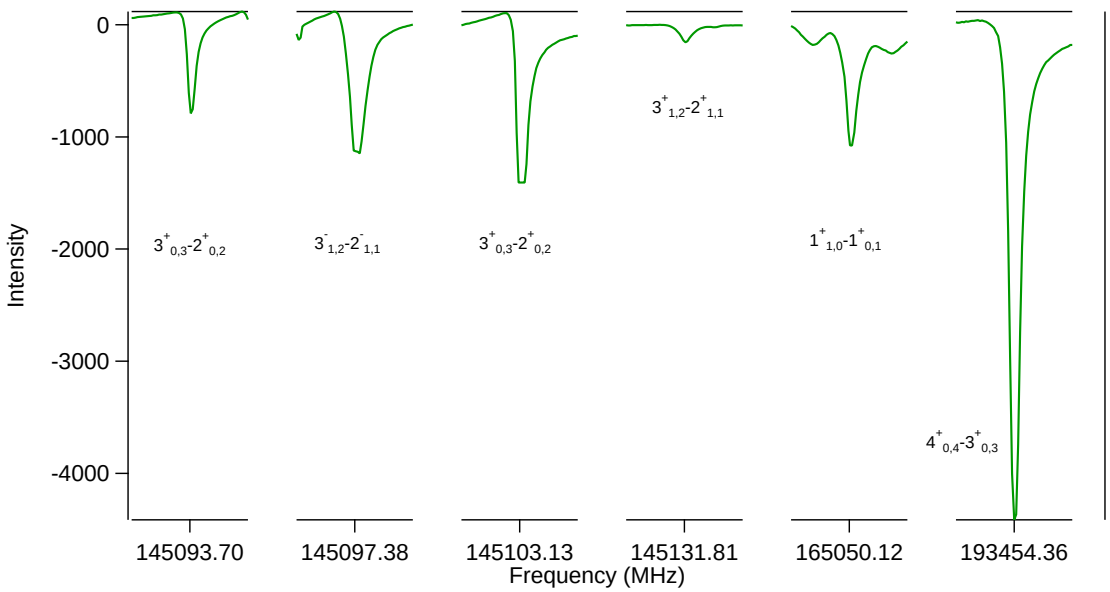

Figure 3.6: Several methanol lines observed after implementation of the multipass optical setup. This figure has been edited from Figure 3 from Reference [22].

right). The baseline stays consistent until the spectral feature, and the effect on the baseline after is unknown, hence the reasoning for picking a region of baseline to the left of the features.

A rotational diagram was created for methanol using the peak intensity approach described. Figure 3.7 shows the rotational diagram constructed using the single peak intensities of each absorption line. The rotational temperature determined from this diagram is 17.2 K $\pm$ 5 K. On the day of this data run, only three methanol lines were collected, by setting up a scan to cover the transitions found at 145,093.754, 145,097.435, and 145,103.185 MHz respectively.

The true number density of molecules cannot be known without intensity calibration, but the y-intercept of a rotational diagram provides reference for further analysis of the relative number density of methanol, and therefore percentage of photolysis products.

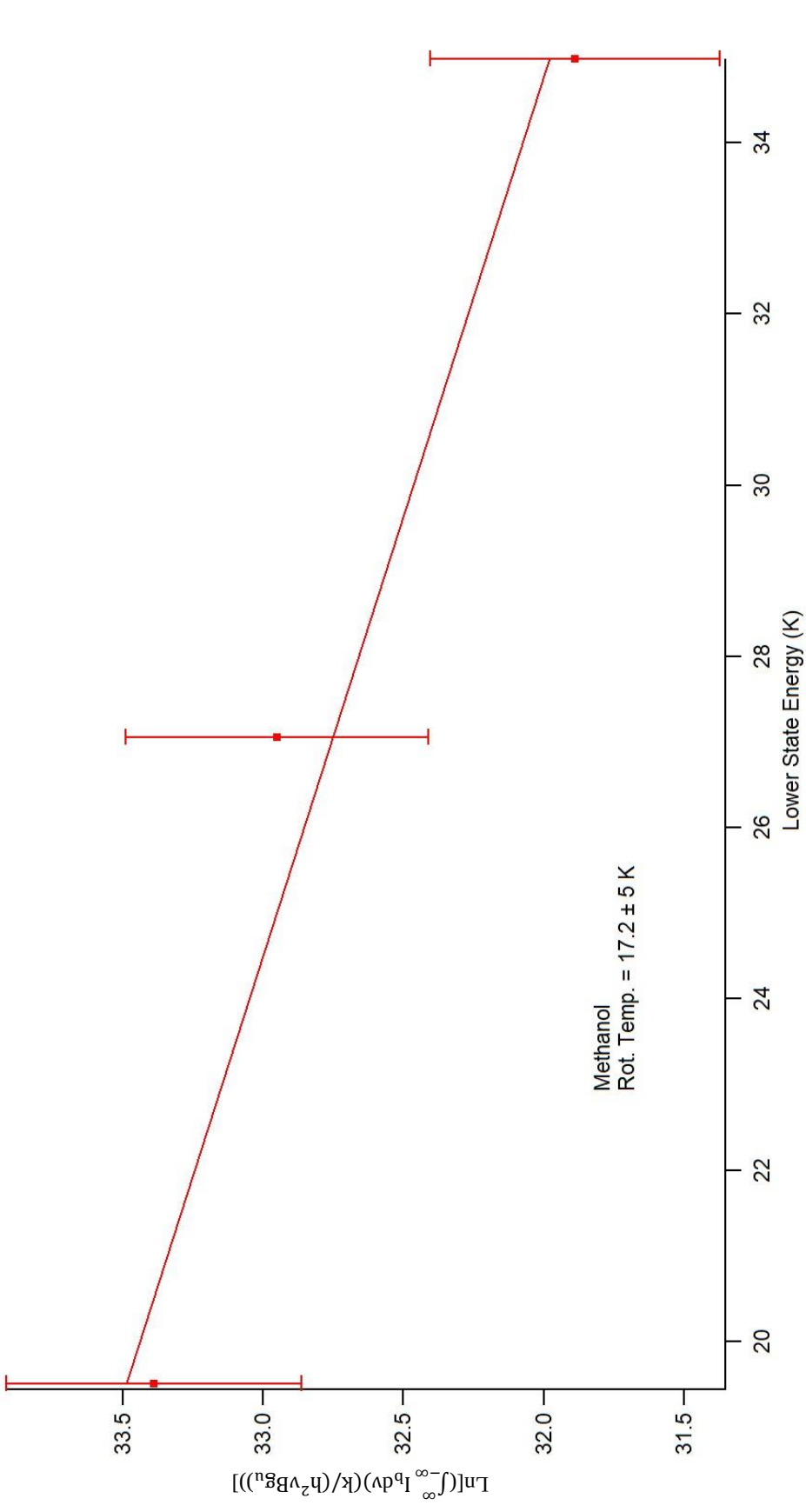

Figure 3.7: The rotational diagram of methanol in the supersonic expansion, calculated using the signal intensity at the peak of the absorption lines.

3.1.4 Improvements to Spectrometer, Detection of Formaldehyde, and Explanations for Asymmetry/Differences in Production

As mentioned in both Chapter 2 and Section 3.1.3, a set of two mirrors were installed in the vacuum chamber to facilitate the creation of a multipass optical system. The multipass allows for the probing mm/submm light to pass through the supersonic expansion a total of seven times, and should lead to an increase in the SNR of collected spectra. Figure 3.8 shows spectra for the methanol absorption line at 145,103.185 MHz before and after implementation of the multipass. Using the ratio of the peak absorption intensity to the RMS noise of each spectrum, the SNR was calculated for each absorption line. The SNR before the multipass was approximately 9, and after the multipass was added the SNR rose to approximately 29, meaning the SNR of spectra produced using the multipass have increased by a factor of 3. These results show that the SNR enhancement was not the factor of 7 that was anticipated; it is likely that the size of the mm/submm beam was large enough that not all of the beam passed through the molecular sample on every pass. Nonetheless, an improvement was observed and so the multipass arrangement was used for all subsequent experiments.

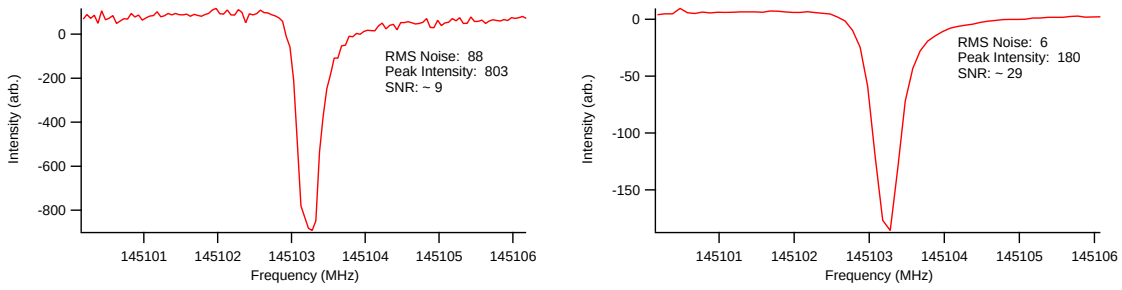

(a) (b)

Figure 3.8: Spectra for the methanol absorption line at 145,103.185 MHz. The peak intensity was measured by taking the y-value of the top of the line, and subtracting the RMS noise value. (a) The methanol absorption spectrum before implementation of the multipass. (b) The methanol absorption spectrum after implementation of the multipass.

The first photolysis product targeted was formaldehyde; as shown by Hagege et al. [15], it is the most stable molecule produced via methanol photolysis, and was seen as a large percentage of the total photolysis products measured in that experiment. An example of formaldehyde spectra taken during methanol photolysis can be seen in Figure 3.9.

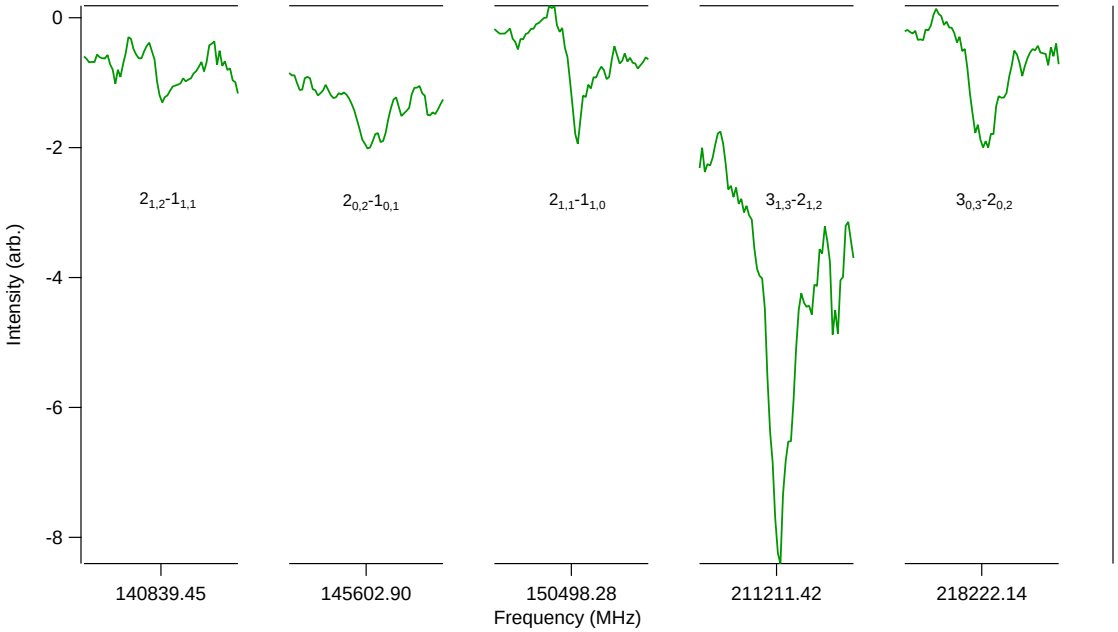

Figure 3.9: Formaldehyde spectra, collected as a result of methanol photolysis. These spectra were collected after implementation of the multipass optical system. This figure has been edited from Figure 6 from Reference [22].

Figure 3.10 shows a closer view of one of the absorption lines detected for formaldehyde as a photolysis product, as well as asymmetry in the line shape; it was also collected before implementation of the multipass optical system.

We found that the amount of formaldehyde produced depends on the position of the laser on the fused silica tube. Theoretical work by Brownsword et al. showed that formaldehyde can be further produced by reactions involving methoxy and hydroxymethyl [23]. Hays et al. summarized these reactions and others in Figure 1.1 [20]. The further down the tube that the UV light was aimed, the less formaldehyde signal was observed. Our current understanding of this phenomenon stems from the colli-

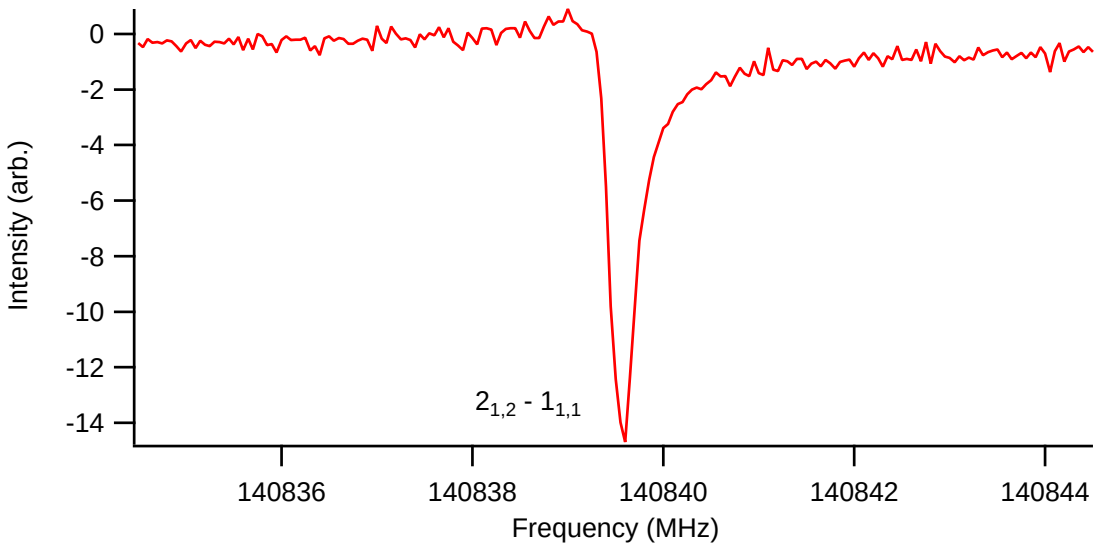

Figure 3.10: A formaldehyde absorption signal detected at 140,839.502 MHz, with the rotational quantum number assignment $2_{1,2}$-$1_{1,1}$.

sions happening in the fused silica tube. As can be seen in Figure 1.1, formaldehyde can either form directly from photolysis, or through further reactions of methoxy and hydroxymethyl. Therefore, formaldehyde is produced in greater concentration when the laser is aimed at the top of the tube, allowing collisions between the radical products in the tube or with the walls of the tube that lead to further reactions. Further discussion on attempting to combat this issue can be found in Section 3.1.8.

3.1.5 Production of Methoxy

While taking the formaldehyde scans, we attempted to search for methoxy radical, which has known rotational lines in the millimeter regime. However, while formaldehyde was prominent, methoxy could not be detected, which seemed odd because of its greater likelihood of being a photolysis product, as shown by Hagege [15]. From the explanations given above, it seemed likely that we were producing methoxy, but it was all reacting away via collisions with the walls of the tube, or other molecules. The first attempts at detecting methoxy using the experimental design depicted in Figure 3.3 yielded no results.

However, during one day of experimental searches, a spectrum was taken centered on a methoxy absorption frequency, in the new configuration described (top of laser beam aligned with bottom of tube), as seen in Figure 3.11. The day this occurred,

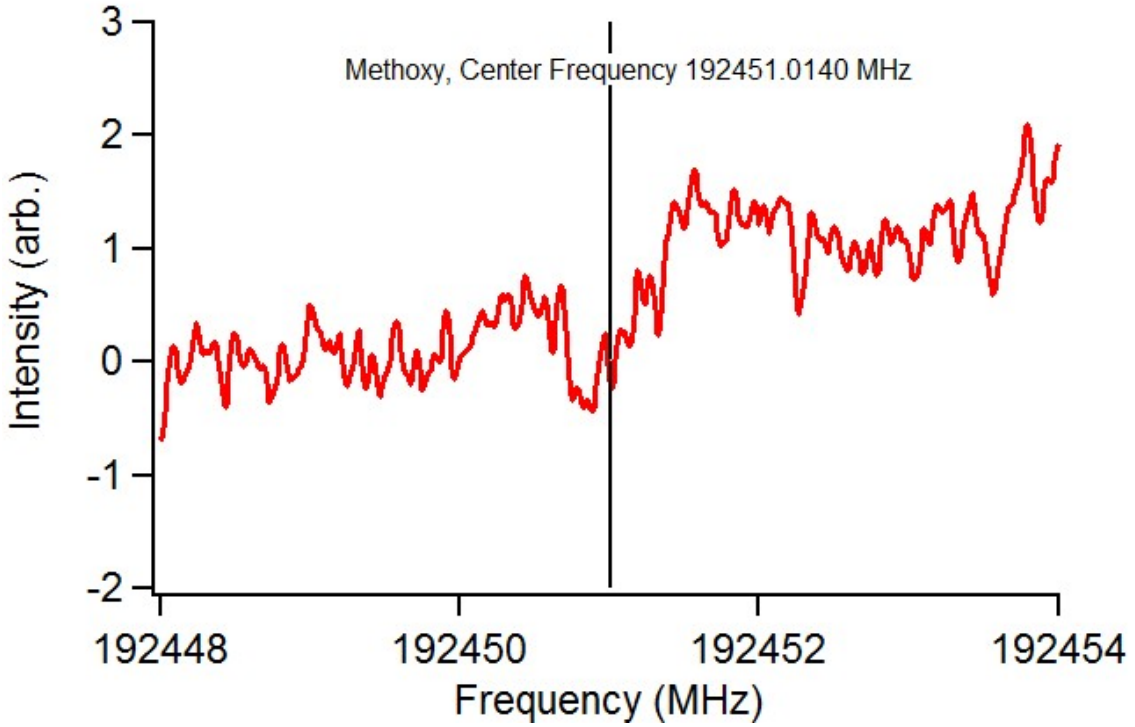

Figure 3.11: A spectrum showing a ground state methoxy transition, collected before implementation of the multipass optical system. This spectrum has been smoothed via boxcar averaging with a filter width of seven.

the pressure behind the pulsed valve was steadily increasing over the course of the 10-hour experiment. While the precise mechanism which led to a rise in the backing pressure is not well understood, it lead to an overall increase in the signal to the point where detection was made possible.

In order to improve the signal to noise ratio on the methoxy signal detected, the multipass setup based on the design used by Kaur et al. [17] was implemented. After incorporating the multipass optics into the spectrometer, we attempted to replicate the conditions under which methoxy was originally detected. Recreating this signal was difficult, and took several months. During a day of experimentation in April of

2017, however, we were able to collect three spectra of of rotationally cold methoxy lines. These spectra can be seen in Figure 3.12. Attempts were made to replicate these

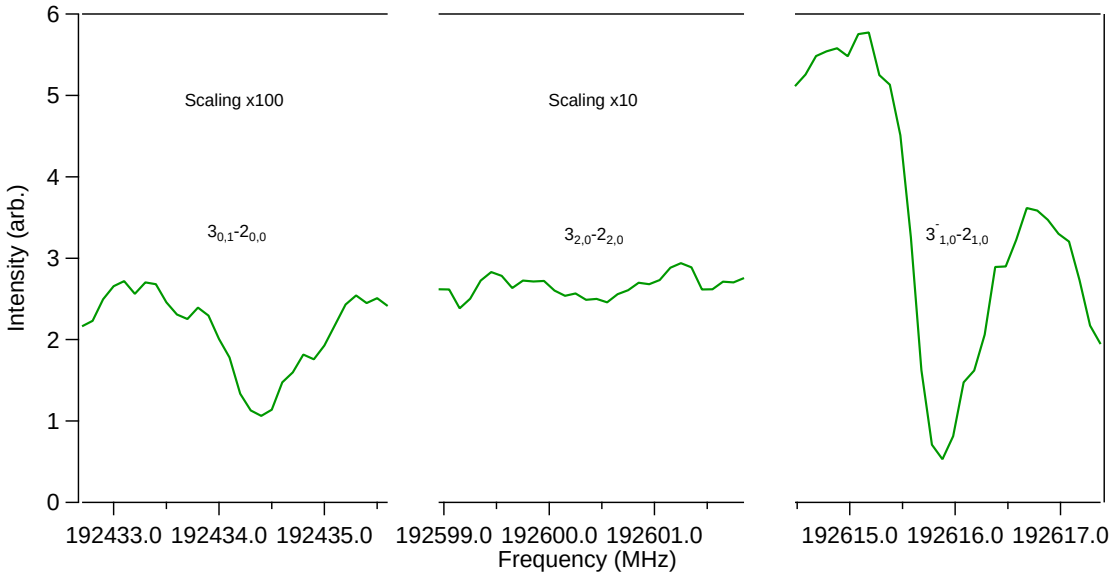

Figure 3.12: Three spectra for methoxy transitions which were collected on the same day. This figure has been edited from Figure 7 from Reference [22].

results under the same experimental conditions, but we were unsuccessful in doing so. Trying to maintain a constant backing pressure over long periods of averaging as well as realigning the laser with the fused silica tube consistently proved to be challenging. We therefore moved on to other experiments to examine whether methoxy might be a minor product of photolysis.

3.1.6 Tentative Hydroxymethyl Detection

In addition to detection of the methoxy radical, we have obtained a preliminary detection of the hydroxymethyl radical, shown in Figure 3.13. Bermudez et al. [24] provided frequencies for rotational transitions of the hydroxymethyl radical that were used to guide our measurements. However, no line strength information was provided in this analysis, and our own fit of their experimental data did not converge. We can therefore only approximate the information needed for the Boltzmann analysis.

From the lines collected in Figure 3.13 and presented in Sections 3.1.3 (Figure 3.6),

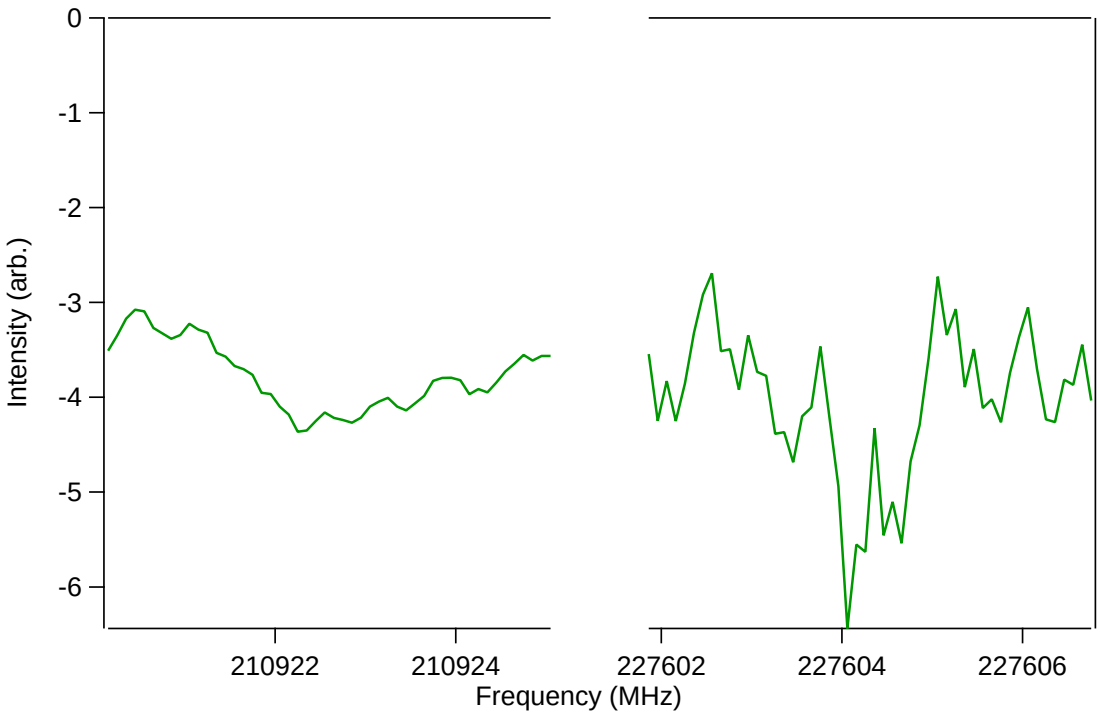

Figure 3.13: Spectra of the radical hydroxymethyl observed as a result of methanol photolysis. This figure has been edited from Figure 8 from Reference [22].

3.1.4 (Figure 3.9), and 3.1.5 (Figure 3.12), we calculated a tentative set of branching ratios for methanol photolysis in the gas and condensed phases, assuming percentages for the methyl branch from the work of both Hagege and Öberg. This information is shown in Table 3.2. The information to produce rotational diagrams for all molecules observed were obtained from the JPL catalogs, except for the hydroxymethyl radical. Bermudez et al. [24] do not provide line strength information for transitions which they observed. They do, however, provide relevant rotational and distortion constants which were used in generating a prediction for a spectrum. We used these constants, and generated our own fit for the spectrum in order to get the relevant partition function and line strength information for the transitions of interest.

Table 3.2: Tentative branching ratios calculated for methanol photolysis in the gas and condensed phases. The methyl branch ratios are assumed from Hagege's and Öberg's results. This table has been edited with permission from Reference [22].

Photolysis Products	Hagege Ratios (gas phase)	Öberg Ratios (condensed phase)	Our Work (gas phase)	Our Work (condensed phase)
Hydroxymethyl (CH_2OH)	75%	73%	53%	49%
Methoxy (CH_3O)	75%	15%	39%	36%
Methyl (CH_3)	<5%	12%	5% (assumed)	12% (assumed)
Formaldehyde (H_2CO)	20%	0%	2%	2%

3.1.7 Implementation of 3D Translation Stage, and Methoxy Raster Tests

It is well known that over long periods of operation, the poppet inside the pulsed valve assembly can wear out, which leads to leaking of the sample, and therefore a change in the backing pressure of the gas mixture. However, we also began to suspect that the tension of the pulsed valve was changing over the course of an experiment. The high repetition rate of pulsing could lead to vibrations, which coupled with gravity, could result in loosening the pulsed valve. The backing pressure prompted us to look for any changes in the pulsed valve during the course of experimentation, and indeed, the pulsed valve orientation relative to the incoming excimer beam would slightly change over the course of eight hours. Aside from the implications this had for the backing pressure (and therefore expansion conditions), this also meant that the photolysis conditions were subject to variation.

To this end, we developed and implemented a 3D translation stage to mount inside the chamber that could be used to align and secure the pulsed valve position. A diagram depicting the stage can be seen in Figure 3.14. The benefits provided by implementation of the 3D translation stage included nearly perfect realignment of the pulsed valve every time it was taken out for repair, with minor adjustments made with

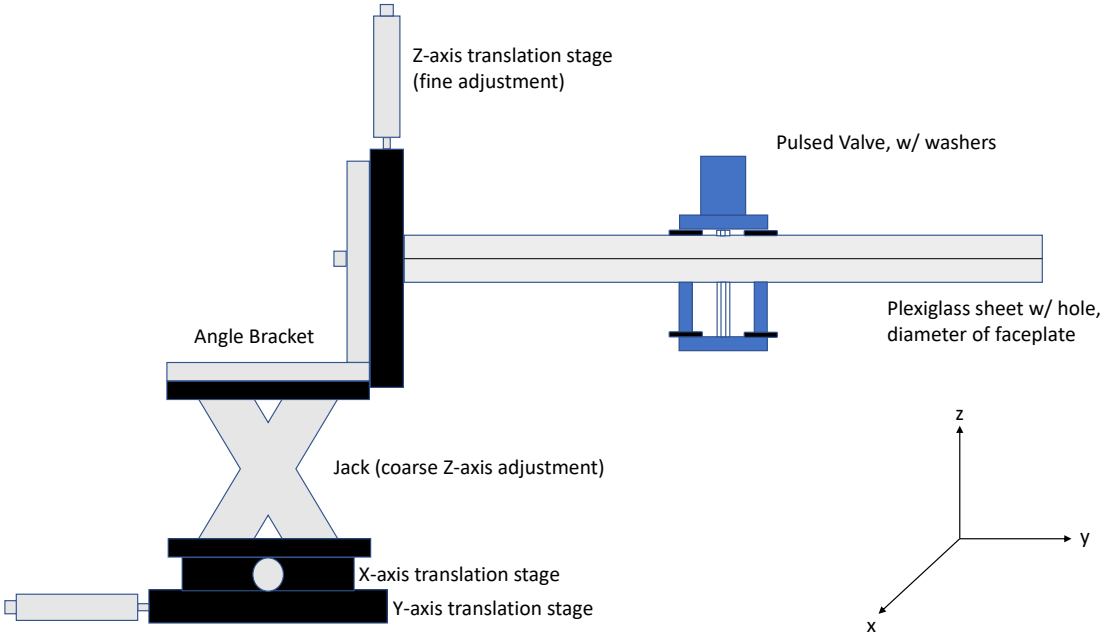

Figure 3.14: The 3D translation stage implemented inside the vacuum chamber.

the translation stages to realign relative to the laser. This alignment reliability also meant that the supersonic expansion, relative to the probing mm/submm radiation, would remain consistent across trials.

In an attempt to characterize the stability offered by the 3D translation stage, a series of tests were performed alongside the tests which will be discussed in Section 3.1.9. Figure 3.15 depicts three methanol lines, collected on five separate days. The methanol bubbler was refilled at the beginning of each day, except for Day 4, where lines were collected when the laser beam profile was 1.5 mm from the bottom of the fused silica tube. It is clear from the spectra collected during these trials that the methanol signal is consistent day-to-day with the exception of Day 4, when the bubbler was not refilled. These tests help to confirm that for the parent molecule, methanol, any signal loss is due to a decrease in sample, and not any instability in the pulsed valve/sample delivery.

In order to test the hypothesis that the differing amounts of photolysis products seen in the experiment depended on the position of the laser beam on the tube, raster

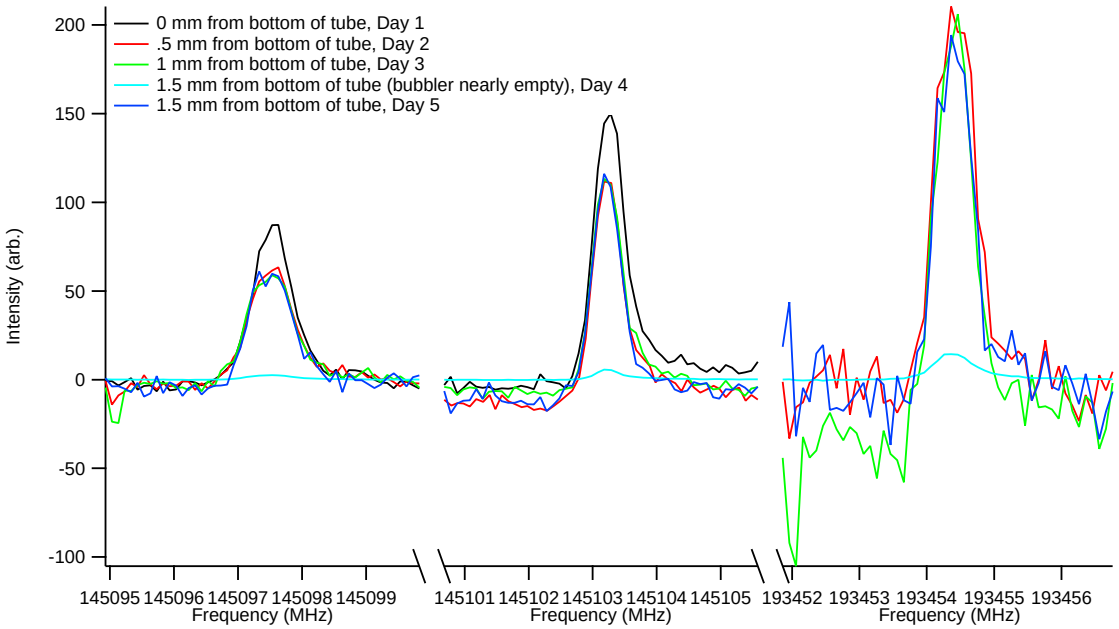

Figure 3.15: Methanol lines which were taken over the course of five days. Failure to fill the methanol bubbler on day four lead to the weak signals for each line at position four, which demonstrates that signal loss is because of a decrease in sample, not pulsed valve stability.

tests were performed. To begin, the top of the laser beam profile (approximately 2 cm in length at the tube) was aligned with the gas channel, a quarter of the way up the tube (1.5 mm). A methanol depletion signal, a formaldehyde photolysis product absorption signal, and a methoxy photolysis product absorption signal were monitored as a function of moving the laser down the fused silica tube. Five positions were tested, with the last position being the top of the rectangular beam profile being flush with the bottom of the tube. A graph depicting the results of these tests can be seen in Figure 3.16. It can be seen in Figure 3.16 that a methoxy signal was observed when the top of the beam profile was 1.5 mm from the bottom of the tube. The signal observed can be seen in Figure 3.17.

After going through the first round of raster tests, the laser was walked back up the fused silica tube, in order to see if the methoxy signal could be replicated. Unfortunately, we could not replicate the signal again; it was decided that if methoxy (or

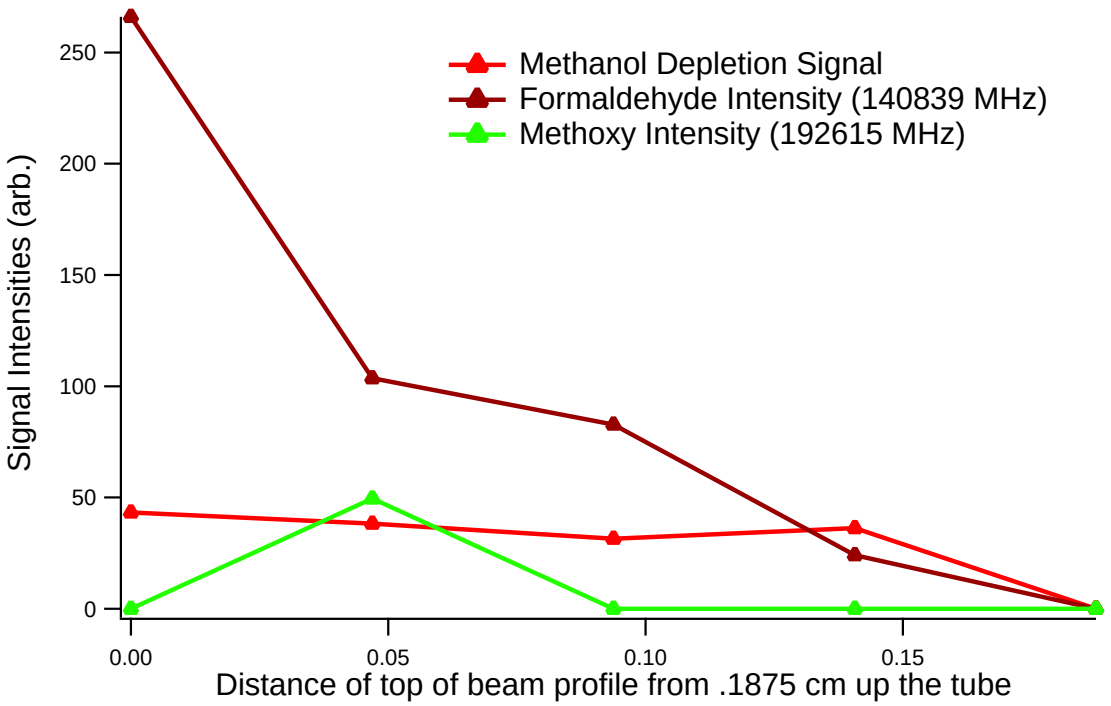

Figure 3.16: A graph showing results of raster tests performed on the fused silica tube.

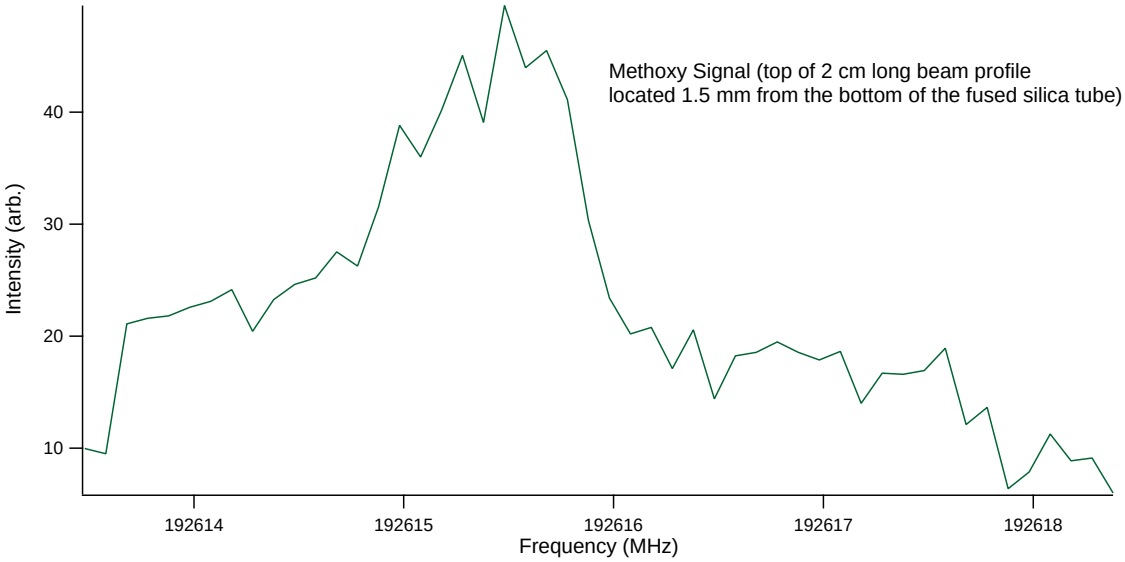

Figure 3.17: The methoxy signal (192,615.9760 MHz) observed when the top of the rectangular beam profile was approximately 1.5 mm away from the bottom of the tube.

anything other than formaldehyde) was being produced by photolysis, more averaging would be required.

While rastering the laser back up the tube (and in conjunction with the scans taken in Figure 3.15), direct absorption scans were taken for formaldehyde signal as a function of laser position on the tube. It is important to note that these raster tests were performed using the spherical focusing lens, rather than the cylindrical focusing lens used for the initial branching ratio tests; more discussion on this changing of optics will be discussed in Section 3.1.8.

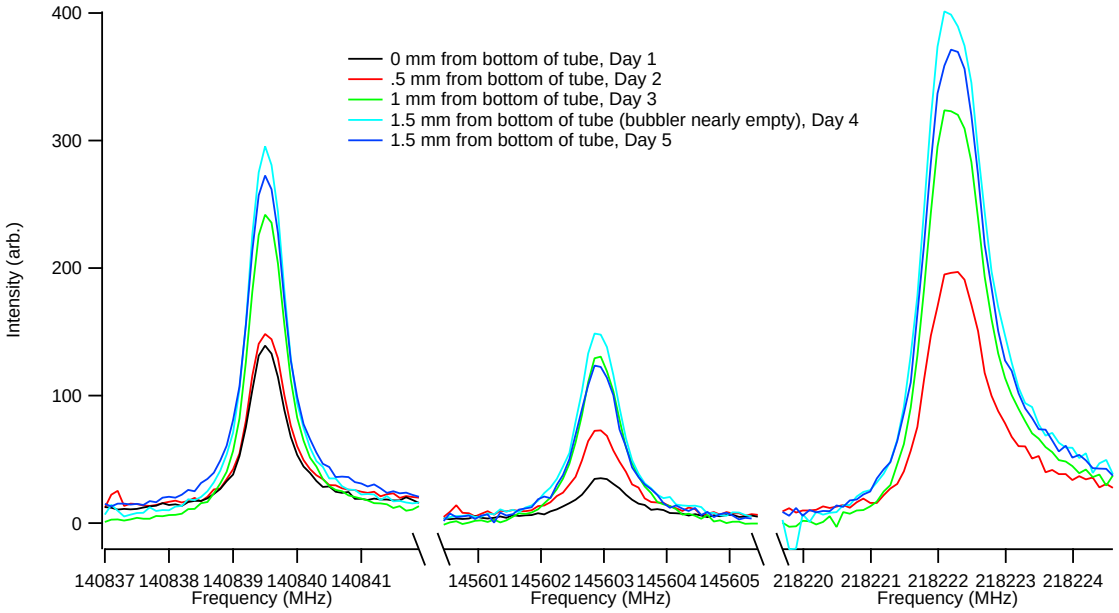

Figure 3.18: Formaldehyde lines which were taken over the course of five days. Raster tests were performed using the spherical focusing lens, which will be discussed in Section 3.1.8.

Formaldehyde production as a function of laser position on the tube is clearly a factor in this experiment, as now shown in Figures 3.16 and 3.18. However, another important piece of information can be gathered from Figure 3.18. As was mentioned in Figure 3.15, the methanol parent signal was the weakest on Day 4. However, for the formaldehyde lines collected on Day 4, the signal was the strongest collected for all three lines; even stronger than the remeasured lines collected on 11/08/17. This result implies that regardless of amount of sample delivered in the supersonic expansion over time, the amount of formaldehyde produced remains virtually the same.

3.1.8 Introduction of Spherical Focusing Lens

After implementation of the 3D translation stage and performing the raster tests, we were still having trouble reliably reproducing radical signal on a day to day basis. We even moved to performing eight hour averages, meaning a total of 24000 averages across a 5 MHz window at 0.1 MHz resolution, versus 2000 averages previously, but we were still unable to reproduce radical signal. It is possible that we were not inducing significant photolysis, due to the cylindrical focusing optic being used. Calculations were performed knowing the laser output energy (16 $\frac{mJ}{pulse}$), the pulse length (8 ns), and the beam size at the focal point of the laser (1 cm^2 for the cylindrical lens, 0.008 cm^2 for the spherical lens). The photon flux calculated for the cylindrical focusing lens is $1.6\times10^{24}\,\frac{\text{photons}}{\text{s}\cdot\text{cm}^2}$, and for the spherical focusing lens it is $2.0\times10^{26}\,\frac{\text{photons}}{\text{s}\cdot\text{cm}^2}$.

The reason for changing the focusing optic from a cylindrical lens to a spherical lens stems from the calculation above. If there are more radicals produced over a larger area within the tube, the probability of collisions between these radicals and other molecules/the walls of the tube is much greater. Performing kinetic molecular theory (KMT) calculations for just the parent molecule methanol knowing the backing pressure of the gas, the inner diameter of the fused silica tube, and the path length the molecules need to travel from the very bottom of the fused silica tube to the aperture exit (0.6 cm), it was calculated that roughly 3720 molecular collisions will occur. Using the spherical focusing lens, photolysis happens over a smaller volume, meaning a decrease in the number of photolysis products, but also a decrease in the number of collisions which may occur, and a greater probability of photolysis occurring in the smaller region. Unfortunately, this might also mean an increased chance of multi-photon absorption for the molecules which do interact with the UV light; this will be discussed further in Section 3.1.10. Regardless, a series of experiments were conducted using the spherical focusing lens; Figures 3.18 and 3.15, seen earlier, were spectra collected after the change in focusing optics.

3.1.9 Detection of Isotopic Formaldehyde

Before creation of the roadmap described in Section 3.1.2, one of the methoxy transitions targeted (based on lower state energy) could be observed at 137,450.5900 MHz. It can be seen from Figure 3.2 that the targeted transition would be very weak compared to some of the others which can be seen closer to the center of the multiplier chain bandwidth. However, over a series of scans performed over 5 days in August 2018, a spectral line was observed near the frequency 137,450 MHz. A single spectrum averaged for 30 minutes can be seen in Figure 3.19. This line (amongst

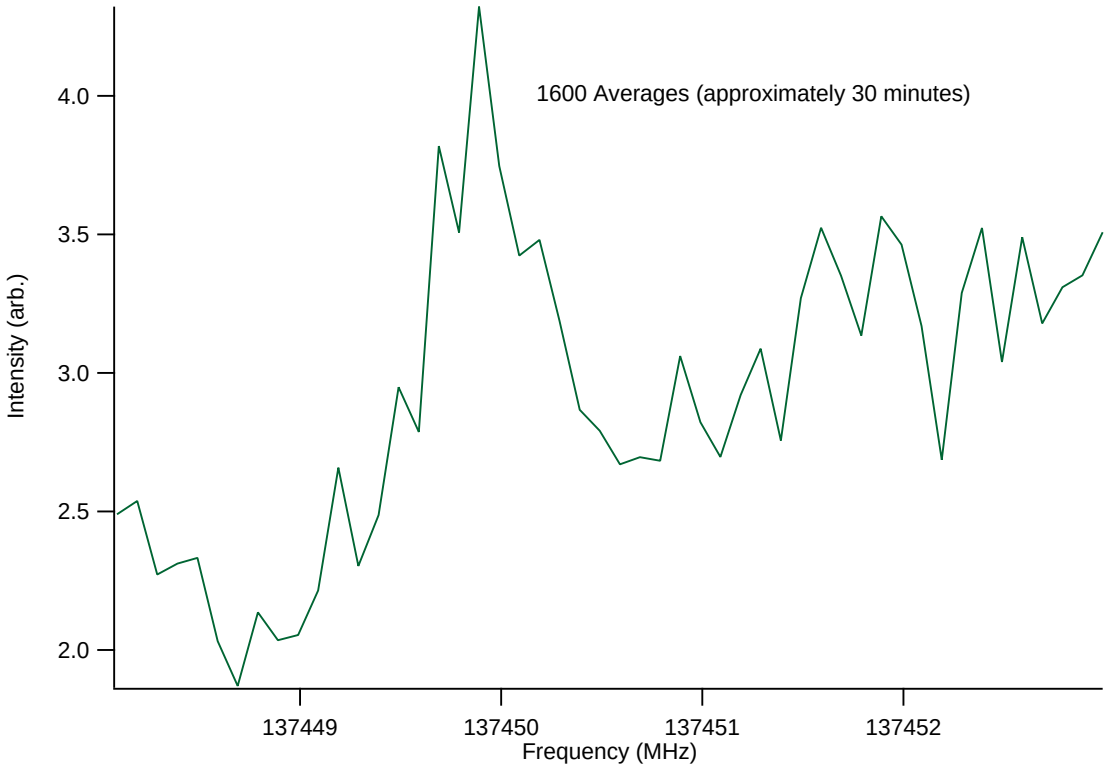

Figure 3.19: A spectrum collected over the course of 30 minutes. It was originally thought to be a methoxy transition, but later analysis revealed it to be a transition for the carbon-13 variant of formaldehyde.

others for other molecules) was averaged over a total of two more hours over the course of four more days, to decrease the amount of noise and confirm there was a line being observed. The averaged spectrum can be seen in Figure 3.20.

Being able to see this signal consistently over the course of five days was a welcome

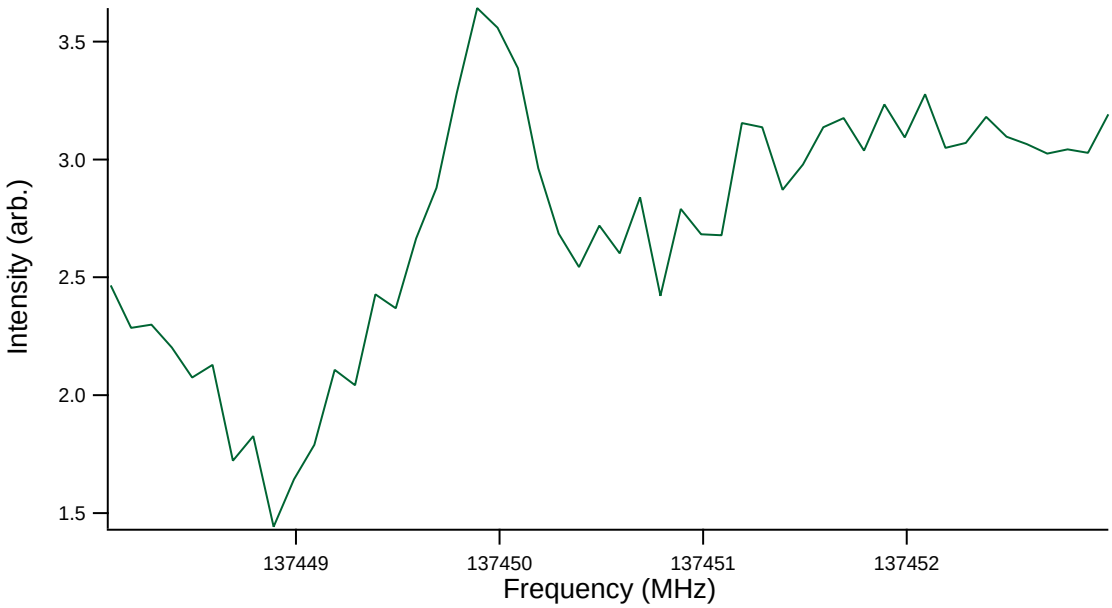

Figure 3.20: The averaged spectrum generated from five spectra collected over the course of five days in August 2018.

sign. It was during these experiments that the roadmap was created, and we realized that it was surprising that we could see any signal at all at this frequency, especially if it was methoxy. To this end, we checked two other methoxy lines at 192,451 and 192,615 MHz, respectively (which are predicted to be very strong on the roadmap). Unfortunately, nothing could really be seen at either frequency; Figure 3.21 shows an example of one of these lines, averaged over the five days.

At this time, we were perplexed; we knew it wasn't methoxy (the line center was about half a MHz off), but there was a clear signal which was being observed. At this time, we consulted Splatalogue[1] in an attempt to figure out which molecule we could be producing that would possess a transition corresponding to the observed spectral line. Searching for lines close to 137,450 MHz, we found a transition that occurs at 137,449.9503 MHz, for the carbon-13 (^{13}C) isotope of formaldehyde. To see if this might be the case, we added the ^{13}C isotope catalog information to the roadmap; this addition, and its comparison to methoxy transitions in the same frequency range,

[1] https://www.cv.nrao.edu/php/splat/

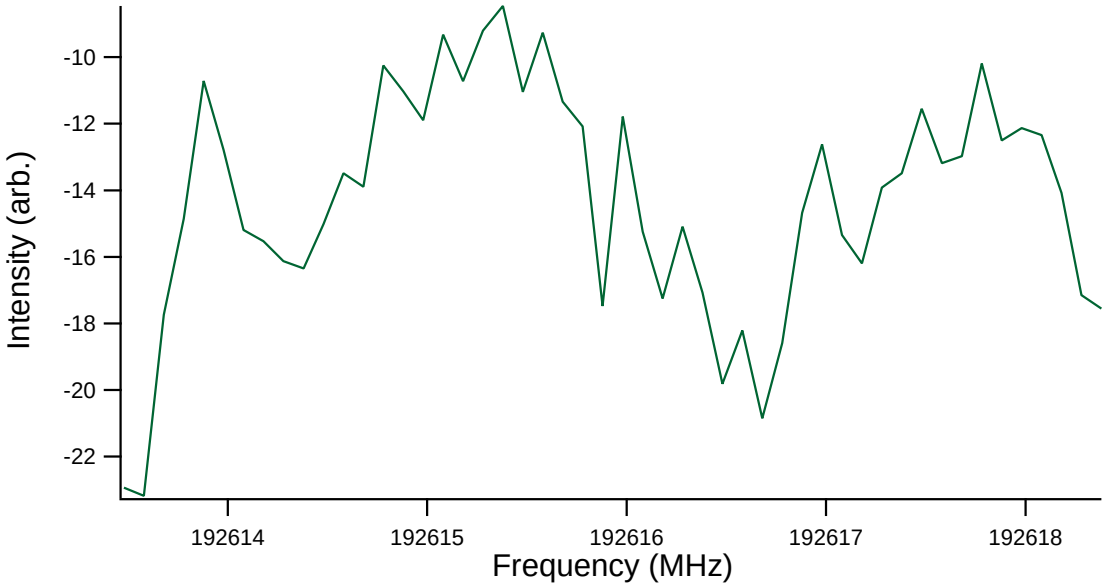

Figure 3.21: An averaged spectrum for a methoxy line which is calculated to be very strong. No discernable signal could be seen after collecting averages during data runs over the course of five days.

can be seen in Figure 3.22. It can be seen that the strongest transitions predicted for isotopic formaldehyde are much stronger than any transitions methoxy would possess in this frequency range, especially around 137,450 MHz. Therefore, a positive detection of ^{13}C formaldehyde was confirmed.

Shortly after these tests, we moved on to the spherical lens raster tests which produced spectra like those seen in Figure 3.18. Over the course of those tests, we also decided to scan for a ^{13}C methanol line, to confirm this theory. The spectra collected can be seen in Figure 3.23.

A small, but noticeable feature can be seen in all five spectra across the five trials. Therefore, there is some small amount of ^{13}C methanol present in natural abundance in our sample, and photolysis of this molecule leads to the production of ^{13}C formaldehyde observed during experimentation.

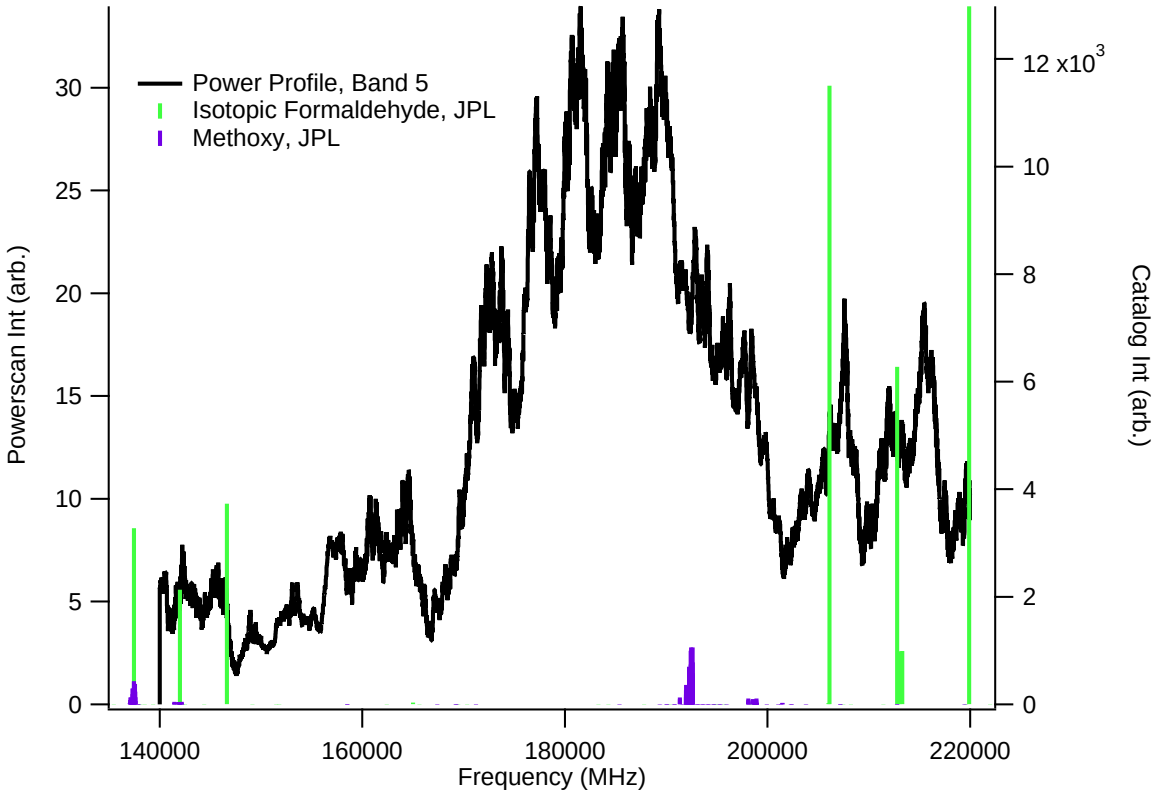

Figure 3.22: A spectrum showing generated intensities for transitions of methoxy and ^{13}C formaldehyde with Q(37.50 K), versus the power profile for Band 5 generated from the AMC-S268 multiplier chain. Arbitrary intensities for the AM power profile and the transitions from the catalog can be found on the left and right vertical axes, respectively.

3.1.10 Detection of CO and H_2O

The final two photolysis products searched for were CO and H_2O, which both have only a handful of accessible rotational lines in the range of our spectrometer. Along with attempting to detect methoxy and hydroxymethyl transitions one last time, three CO transitions and two water transitions were investigated.

While investigating water as a photolysis product, a discovery was made about the nature of detecting water in this experiment. Figure 3.24 shows a comparison between measuring methanol in the chamber versus water in the chamber, when the pulsed valve is on or off. It can be seen in Figure 3.24(a) that the methanol signal is much higher when sample is present. However, the opposite is true for water; Figure 3.24(b)

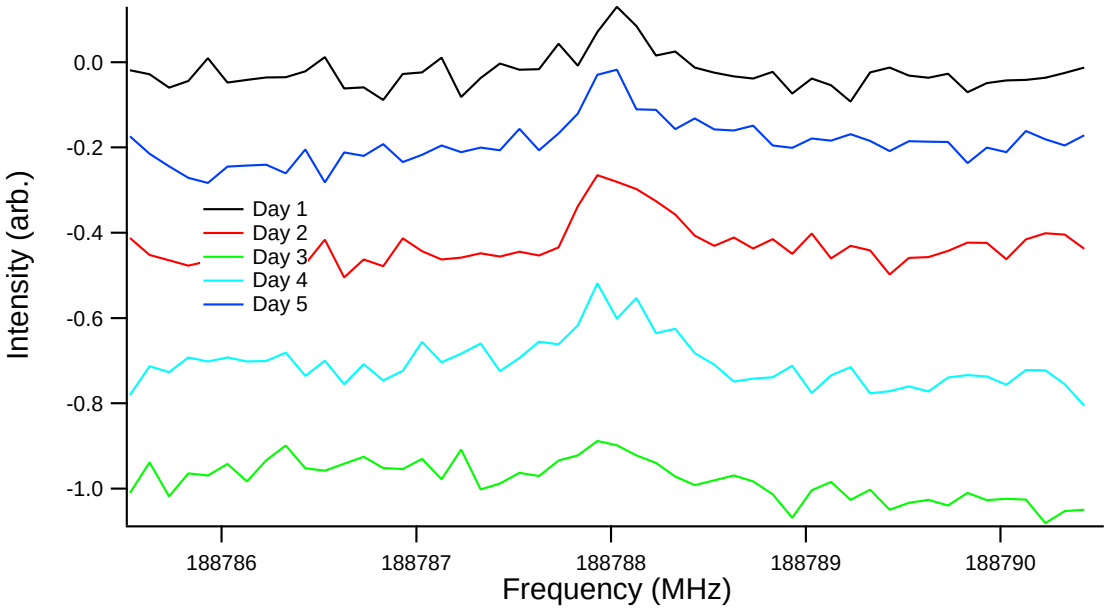

Figure 3.23: C-13 methanol spectra collected during the course of the spherical lens raster tests. A weak spectral line can be seen around the line center given in the CDMS catalog, 188,788.029 MHz.

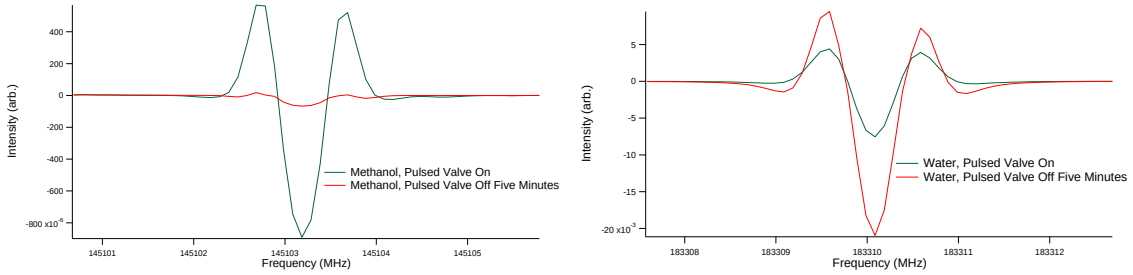

(a) (b)

Figure 3.24: Spectra comparing the amounts of molecules in the path of the mm/submm radiation, while the pulsed valve is operational, and five minutes after the pulsed valve has ceased operation. (a) A methanol absorption signal observed while the pulsed valve is operational, and five minutes after the pulsed valve has ceased operation. (b) A water absorption signal observed while the pulsed valve is operational, and five minutes after the pulsed valve has ceased operation.

shows that water absorption is higher when the valve is off, rather than when it is pulsing sample into the chamber. We attribute this to some amount of atmospheric water which is constantly present in the vacuum chamber. When the valve is pulsing, even if photolysis is being conducted on the methanol in the expansion, the water signal will always be lower than when the supersonic expansion is not present. This

is presumably because the expansion displaces the atmospheric water molecules out of the path of the mm/submm radiation. This was a concern for the first water line targeted that had a lower state energy of 136 cm^{-1}, or 194 K. To route around this problem, we targeted another water transition with a lower state energy of 34 K that would presumably only be strong when seen in the expansion.

Figure 3.25 shows a water spectrum collected when no methanol was present; no observable signal is detected, meaning atmospheric water leaking into the chamber would not obfuscate any result collected when the methanol was being pulsed. Next, we conducted tests with the sample pulsing, and alternating averaging with the laser on and off each hour, for a total of four hours. Figure 3.26 compares the spectra collected. The results seemed odd between hour one and two of averaging for either set of spectra; to get a better picture of how the signal was evolving, Figure 3.27 shows the evolution of the water signal with time.

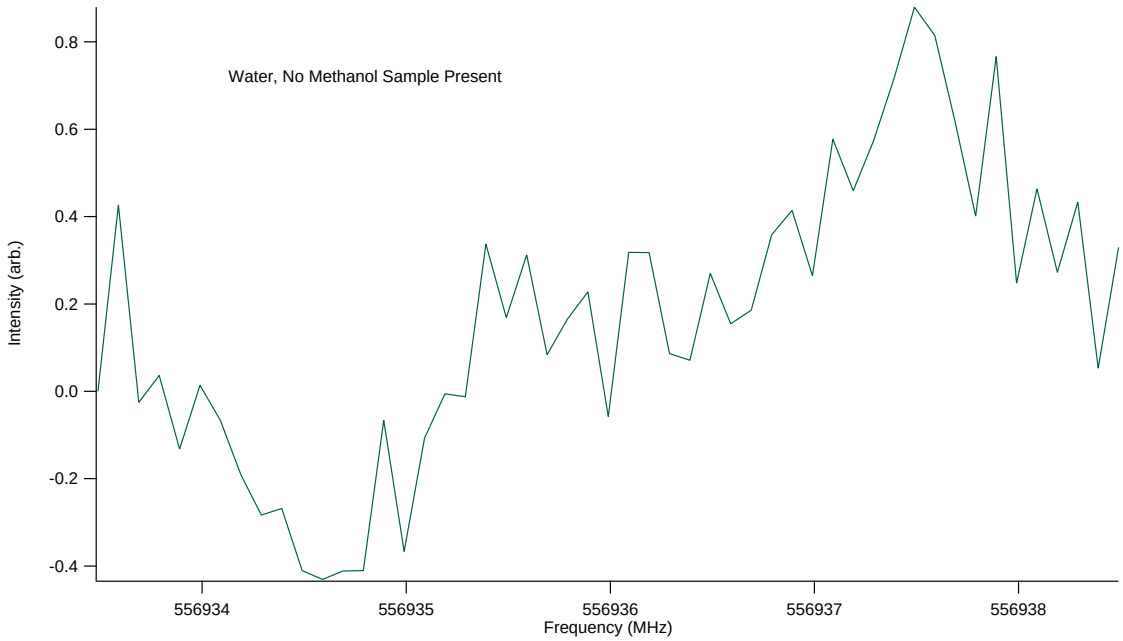

Figure 3.25: A spectrum collected around the line center for the water transition of interest. No observable signal could be seen.

As a function of time, there is a steady depletion of the water signal observed. This indicates that it is atmospheric water from the bubbler, or water impurity from

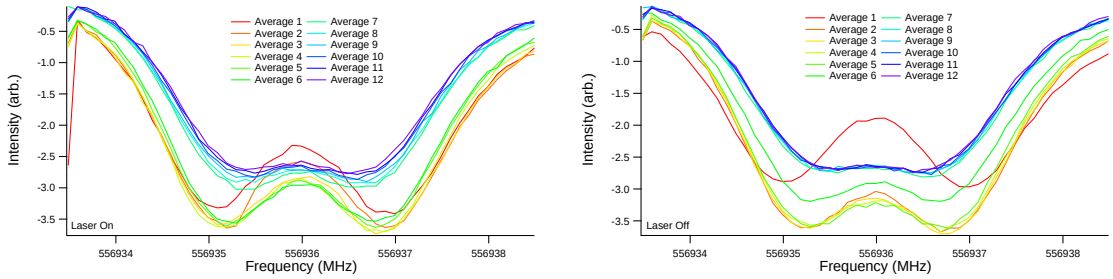

(a) (b)

Figure 3.26: Spectra comparing the water signal observed through twelve acquisitions with the laser on, and another twelve with the laser off. (a) Twelve acquisitions over the water line, collected while the excimer laser was pulsing. (b) Twelve acquisitions over the water line, collected while the excimer laser was off.

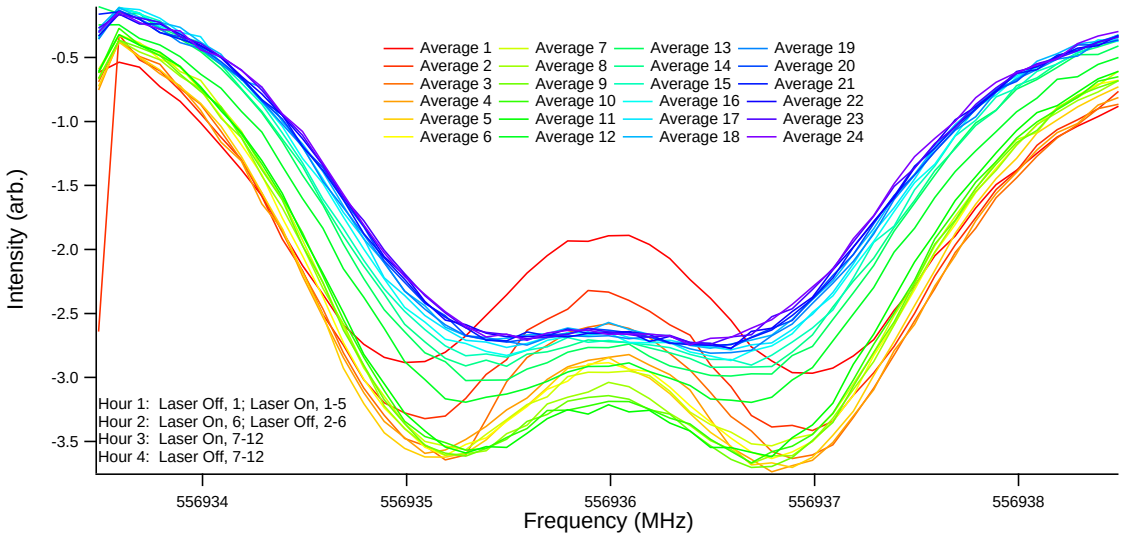

Figure 3.27: The spectra collected for the water transition collected when the laser was on and off. The color scheme for the plot (from red to violet) shows the chronological evolution of the water signal. The depletion of the signal with respect to time, and irregardless of whether the laser was pulsing or not, seems to indicate the water observed was a contaminant in the sample.

the sample. Over the course of four hours, the water signal decreased consistently, meaning that the atmospheric water was slowly being pumped out of the sample. Unfortunately, the amount of water which was present makes it difficult to claim whether water was being produced as a photolysis product or not. In the future, if we are to try and observe water, this problem must be dealt with.

After implementation of the spherical focusing lens, we attempted to search for

radical lines one more time, averaging on three methoxy transitions and one hydroxymethyl transition for eight hours apiece. We did not see any radical production in this new configuration, and so we moved on to the final product we were going to search for, carbon monoxide.

We performed four hours of averaging apiece on three different CO transitions. These scans were evaluated using a program written in Python by Dr. Luyao Zou to perform polynomial baseline fitting/subtraction, as well as fitting Gaussian lineshapes to the spectra. Of the three transitions, only one showed a spectral feature. Figure 3.28 shows the baseline subtracted CO spectrum.

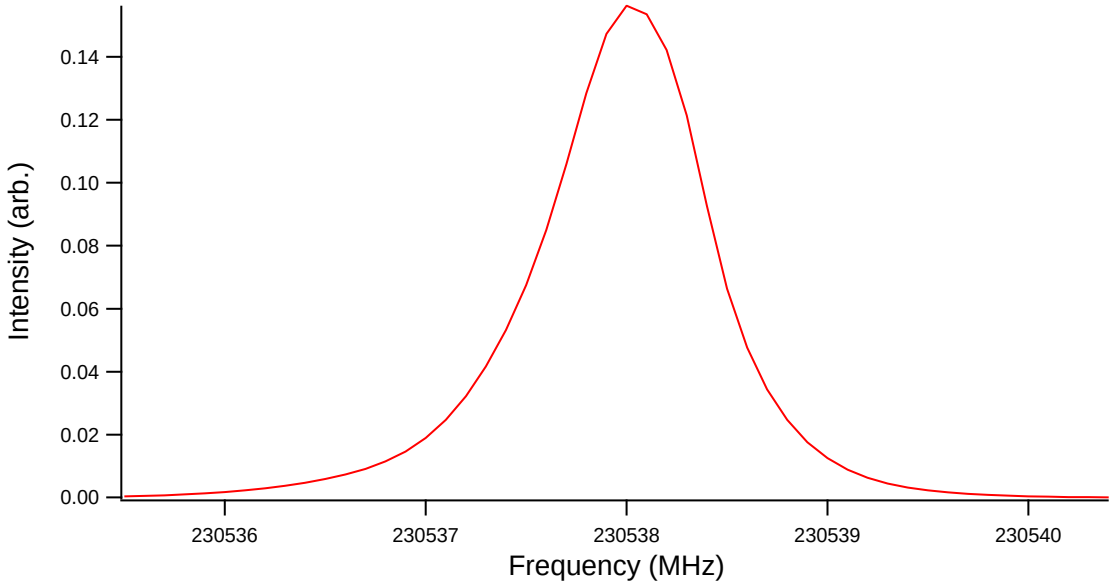

Figure 3.28: The baseline subtracted, averaged spectra for the CO transition observed.

Very early in this project while the cylindrical focusing lens was still being used for the UV beam, we attempted to find CO, but could not see it. Now that we have switched to the spherical lens, it is clearly observed at high SNR. One explanation for the production of this molecule may be due to multiphoton processes. Anderson et al. [25] found that for small molecules like methanol, multiphoton dissociation increased as a function of the laser radiant energy fluence, as well as the reactant pressure (meaning an increased number of collisions for the parent molecule). Because the

Table 3.3: Branching Ratios and number densities/upper limits calculated for various photolysis products from scans performed with the spherical focusing lens.

Molecule	Branching Ratio	Number Density (molecules/cm^2)
Formaldehyde	72%	$2.57*10^{17}$
Carbon Monoxide	2%	$6.67*10^{15}$
Methoxy	N/A	$< 3.73*10^{16}$
Hydroxymethyl	N/A	$< 6.90*10^{15}$
Water	N/A	$< 1.10*10^{14}$

photon flux for the spherical focusing lens is much higher than that of the cylindrical focusing lens, even though the sample pressure is the same, the probability of multiphoton absorption is higher, meaning an increased production of non-condensable molecules, like CO and H_2.

Another set of fitting branching ratios for the formaldehyde and CO observed was calculated for this experiment, and upper limits were found for the methoxy, hydroxymethyl, and water channels as well. The results can be seen in Table 3.3. From the rotational diagram created for formaldehyde, and assuming about 1% of the total methanol is photolyzed ($3.57*10^{17} \frac{molecules}{cm^2}$), roughly 72% of the total photolysis products from the number density for methanol calculated is formaldehyde. From the intensity information gathered for the one CO line observed, only 2% of the photolysis products are calculated to be CO. All other number densities were determined from fitting the RMS value of the noise around where the line centers would be found.

3.1.11 Future Directions

The future of the methanol photolysis project will focus on addressing existing issues, as well as the collection of spectra for molecules which have and have not been observed yet. The atmospheric water contaminant in the methanol bubbler must dealt with in a fashion that will not detract from the amount of parent molecule in the bubbler, before the experiment has even begun. The potential multiphoton absorption issue may be dealt with in the future by implementation of neutral density filters in front of the spherical focusing lens in an effort to decrease the photon flux

at the site of photolysis.

The recent acquisition of two high-frequency multiplier chains from Dr. Stefanie Milam, with frequency ranges of 1825-1975 GHz and 2500-2600 GHz, respectively, allow for the potential to probe for three hydroxyl (OH) radical transitions. New students in the Widicus Weaver lab are currently testing the multiplier chains to characterize their functionality, and planning to perform these experiments in the near future.

Chapter 4 Conclusions

The photolysis of methanol using the spectrometer design described in Section 2 has been performed. Initial detections of the photolysis products methoxy and hydroxymethyl have been collected, and a set of tentative branching ratios has been calculated using this information. Implementation of a new scheme to secure the source alignment, and the subsequent improvements to experimental stability have been observed. Implementation of a spherical focusing lens for the UV light, and the detection of the ^{13}C variant of formaldehyde produced as a result of laser photolysis, as well as carbon monoxide have been shown. In both experiments, H_2CO was found to be a dominant channel in methanol photodissociation at 193 nm. Additional experiments exploring the influence of UV flux on the resultant chemistry, as well as searches for the OH channel, will be conducted in the future.

Bibliography

1. 871, O. S. U. A. *Introduction to the Interstellar Medium* http://www.astronomy.ohio-state.edu/~pogge/Ast871/Notes/Intro.pdf. [Online; accessed 20-October-2016]. 2003.
2. Garrod, R. T., Weaver, S. L. W. & Herbst, E. Complex Chemistry in Star-forming Regions: An Expanded Gas-Grain Warm-up Chemical Model. *The Astrophysical Journal* **682,** 283 (2008).
3. Tennyson, J. *Molecules in Space* http://www.ucl.ac.uk/phys/amopp/people/jonathan_tennyson/papers/311.pdf. [Online; accessed 20-October-2016]. 2003.
4. Charnley, S. B., Kress, M. E., Tielens, A. G. G. M. & Millar, T. J. Interstellar Alcohols. *The Astrophysical Journal* **448,** 232 (07/1995).
5. Herbst, E., Green, S., Thaddeus, P. & Klemperer, W. Indirect observation of unobservable interstellar molecules. *The Astrophysical Journal* **215,** 503 (07/1977).
6. Millar, T. J., Herbst, E. & Charnley, S. B. The formation of oxygen-containing organic molecules in the Orion compact ridge. *The Astrophysical Journal* **369,** 147 (03/1991).
7. Horn, A. *et al.* The Gas-Phase Formation of Methyl Formate in Hot Molecular Cores. *The Astrophysical Journal* **611,** 605–614 (08/2004).
8. Laas, J. C., Garrod, R. T., Herbst, E. & Weaver, S. L. W. Contributions from Grain Surface and Gas Phase Chemistry to the Formation of Methyl Formate and Its Structural Isomers. *The Astrophysical Journal* **728,** 71 (01/2011).
9. Garrod, R. T. A Three-phase Chemical Model of Hot Cores: The Formation of Glycine. *The Astrophysical Journal* **765,** 60 (02/2013).
10. Cheung, A. C., Rank, D. M., Townes, C. H., Thornton, D. D. & Welch, W. J. Detection of NH3Molecules in the Interstellar Medium by Their Microwave Emission. *Physical Review Letters* **21,** 1701–1705 (12/1968).
11. Gibb, E. L., Whittet, D. C. B., Boogert, A. C. A. & Tielens, A. G. G. M. Interstellar Ice: TheInfrared Space ObservatoryLegacy. *The Astrophysical Journal Supplement Series* **151,** 35–73 (03/2004).
12. Chang, A. & Lin, S. A theoretical study of the $O(^1D) + \{CH_4\}$ reaction {II}. *Chemical Physics Letters* **384,** 229–235. ISSN: 0009-2614 (2004).
13. Xia, W. S., Zhu, R. S., Lin, M. C. & Mebel, A. M. Low-energy paths for the unimolecular decomposition of CH_3OH: A G2M/statistical theory study. *Faraday Discuss.* **119,** 191–205 (0 2002).

14. Ing, W. C., Sheng, C. Y. & Bozzelli, J. W. Development of a detailed high-pressure reaction model for methane/methanol mixtures under pyrolytic and oxidative conditions and comparison with experimental data. *Fuel Processing Technology* **83,** 111–145 (09/2003).

15. Hagege, J., Roberge, P. C. & Vermeil, C. Collision-induced predissociation in the gas phase. Photolysis of methanol at 1849 A. *Trans. Faraday Soc.* **64,** 3288–3299 (0 1968).

16. Öberg, K. I., Garrod, R. T., van Dishoeck, E. F. & Linnartz, H. Formation rates of complex organics in UV irradiated CH_3OH-rich ices. *Astronomy & Astrophysics* **504,** 891–913 (07/2009).

17. Kaur, D. *et al.* Multipass cell for molecular beam absorption spectroscopy. *Appl. Opt.* **29,** 119–124 (01/1990).

18. Laas, J. C., Hays, B. M. & Widicus Weaver, S. L. Multipass Millimeter/Submillimeter Spectrometer to Probe Dissociative Reaction Dynamics. *The Journal of Physical Chemistry A* **117.** PMID: 23678971, 9548–9554 (2013).

19. Pickett, H. *et al.* Submillimeter, Millimeter, and Microwave Spectral Line Catalog. *Journal of Quantitative Spectroscopy and Radiative Transfer* **60,** 883–890 (11/1998).

20. Hays, B. M. *et al.* Rotational spectral studies of O(1D) insertion reactions with methane and ethylene: Methanol and vinyl alcohol in a supersonic expansion. *Chemical Physics Letters* **630,** 18–26. ISSN: 0009-2614 (2015).

21. McCabe, M. N. *Understanding Interstellar Chemistry: A Look at Methanol Branching Ratios and the Search for Aminomethanol* MA thesis (Emory University, 05/2016).

22. Weaver, S. W., Powers, C., McCabe, M. & Zinga, S. *Laboratory Measurements of Methanol Photolysis Branching Ratios to Guide Astrochemical Models* in *Proc. of: Astrochemistry VII: Intl. Astronomical Union Symp.* (2017).

23. Brownsword, R. A., Hillenkamp, M., Schmiechen, P., Volpp, H.-R. & Upadhyaya, H. P. Absolute Reactive Cross Section for H Atom Formation in the Reaction of Translationally Energetic $O(^1D)$ Atoms with Methane. *The Journal of Physical Chemistry A* **102,** 4438–4443 (1998).

24. Bermudez, C., Bailleux, S. & Cernicharo, J. Laboratory detection of the rotational-tunnelling spectrum of the hydroxymethyl radical, CH_2OH. *Astronomy & Astrophysics* **598,** A9 (01/2017).

25. Anderson, D., Mcaupine, R. D., Evans, D. & Adams, H. A comparison of the HF laser-induced multiphoton decomposition of methanol and 2,2,2-trifluoroethanol. *Chemical Physics Letters* **79,** 337–343 (04/1981).